

Explaining Low Energy γ -ray Excess from the Galactic Centre using a Two Component Dark Matter Model

Anirban Biswas¹

*Astroparticle Physics and Cosmology Division,
Saha Institute of Nuclear Physics, Kolkata 700064, INDIA²*

ABSTRACT

Over the past few years, there has been a hint of the γ -ray excess observed by the Fermi-LAT satellite borne telescope from the regions surrounding the Galactic Centre at an energy range ~ 1 -3 GeV. The nature of this excess γ -ray spectrum is found to be consistent with the γ -ray emission expected from dark matter annihilation at the Galactic Centre while disfavoured other known astrophysical sources as the possible origin of this phenomena. It is also reported that the spectrum and morphology of this excess γ -rays can well be explained by the dark matter particles having mass in the range 30 \sim 40 GeV annihilating significantly into $b\bar{b}$ final state with an annihilation cross section $\sigma v \sim (1.4 - 2.0) \times 10^{-26}$ cm³/s at the Galactic Centre. In this work, we propose a two component dark matter model where two different types of dark matter particles namely a complex scalar and a Dirac fermion are considered. The stability of both the dark sector particles are maintained by virtue of an additional local $U(1)_X$ gauge symmetry. We find that our proposed scenario can provide a viable explanation for this anomalous excess γ -rays besides satisfying all the existing relevant theoretical as well as experimental and observational bounds from LHC, PLANCK and LUX collaborations. The allowed range of “effective annihilation cross section” of lighter dark matter particle for the $b\bar{b}$ annihilation channel thus obtained is finally compared with the limits reported by the Fermi-LAT and DES collaborations using data from various dwarf spheroidal galaxies.

¹email: anirban.biswas@saha.ac.in

²Present address: Harish-Chandra Research Institute, Chhatnag Road, Jhusi, Allahabad, 211019, INDIA

1 Introduction

The existence of the dark matter (DM) in the Universe is now an established fact by various astronomical measurements and observations such as galaxy rotation curves, gravitational lensing of distant objects, Bullet cluster etc. However, no information is still available to us about the nature and the constituents of dark matter. The most successful hypothesis until now is that the dark matter of the Universe is composed of Weakly Interacting Massive Particles or WIMPs. The particle nature of the dark matter can be explored mainly in two ways. One of them is the process of direct detection where the information about the mass of the dark matter candidate along with its scattering cross section off the detector nuclei can be obtained by measuring the recoil energy of the latter as a result of scattering of the dark matter particles with the nuclei. The DM particles may also be trapped gravitationally within the massive celestial objects like the Sun, Earth etc. in case their escape velocities fall short of that required to overcome the gravity at the central regions of these heavenly bodies. Moreover, the centre of our Milky way galaxy is also enriched with huge amount of dark matter. Annihilation of these trapped dark matter particles can result in the production of high energy neutrinos, positrons (particle antiparticle pair in general), γ -rays etc. Detection of such annihilation products will provide valuable information about the constituents of the dark matter in the Universe. This is known as the process of indirect detection. More information about the properties of WIMPs and their detection procedures (both direct and indirect) are discussed in Refs. [1,2].

It has been claimed by several groups [3–10] in last few years after analysing the Fermi-LAT data [11] that a hint of the γ -ray excess has been observed by the Fermi-LAT satellite borne telescope [12] from the regions surrounding the Galactic Centre (GC) at an energy range ~ 1 -3 GeV. More recent analyses of Fermi-LAT data by Daylan et. al. [10] have disfavoured the possibilities of its astrophysical origin and strongly indicating that the spectrum of this anomalous excess γ -rays is consistent with the emission expected from dark matter annihilation at the Galactic Centre. It is also reported in the same article [10] that the observed γ -ray spectrum can be well explained by a dark matter particle having mass in the range ~ 30 -40 GeV (or ~ 7 -10 GeV) and annihilating significantly into $b\bar{b}$ (or $\tau^+ \tau^-$) final state with an annihilation cross section $\sigma_{v_{b\bar{b}}} \sim (1.4 - 2.0) \times 10^{-26} \text{ cm}^3/\text{s}$ ³. Although, there are some previous works [13–32] where different particle dark matter models have been proposed to explain this low energy (GeV scale) γ -ray excess from the neighbourhood regions of the Galactic Centre but in most of these articles the authors have considered single component dark matter model *i.e.* all the dark matter

³annihilation into $\tau^+ \tau^-$ final state the required cross section is $\sigma_{v_{\tau^+\tau^-}} \sim 2.0 \times 10^{-27} \text{ cm}^3/\text{s}$ (with local dark matter density = $0.4 \text{ GeV}/\text{cm}^3$) for a $\sim 10 \text{ GeV}$ DM particle [8].

present in the Universe are constituted by a single stable beyond Standard Model particle. The larger dark matter mass ranges which also give acceptable fits to the Fermi-LAT data for the $b\bar{b}$ annihilation channel are discussed in Refs. [33,34]. A nonthermal decaying dark matter scenario explaining the anomalous γ -ray excess from the GC is shown in Ref. [35].

The Standard Model (SM) of particle physics does not contain any stable particle which can play the role of DM. Therefore it is generally assumed, in the existing literature, that the observed relic density of the entire dark sector is contributed by a single beyond SM particle. However, there are reasons to believe that the dark sector may also possess some diversity in its particle spectrum like the visible sector of our Universe. One of the major reasons is the similarity between the observed abundances of both the dark and visible sector at the present epoch. Recently, various multicomponent dark matter models have been studied by several groups [36–42]. In this present work, our endeavour is to explore the possibility of having multicomponent DM scenario and study whether it can provide a viable explanation of the Fermi-LAT observed γ -ray excess from the regions close to the GC while simultaneously satisfying all the existing theoretical, experimental as well as the observational bounds.

We propose a two component dark matter model where the dark sector is composed of two different types of particles namely, a complex scalar (S) and a Dirac fermion (ψ). Our proposed model is an extension of the Standard Model of particle physics where the scalar sector of the SM is enlarged by the two SM gauge ($SU(3)_c \times SU(2)_L \times U(1)_Y$) singlet complex scalar fields S and Φ_s . The stability of these dark sector particles are ensured by the application of an additional local $U(1)_X$ gauge symmetry under which only the two dark sector particles S , ψ and the complex scalar Φ_s transform nontrivially. Therefore, the Lagrangian of this present two component dark matter model remains invariant under the $SU(2)_L \times U(1)_Y \times U(1)_X$ gauge symmetry which breaks spontaneously to a residual $U(1)_{em} \times \mathbb{Z}_2$ symmetry when the complex scalars Φ (usual SM Higgs doublet) and Φ_s acquire Vacuum Expectation Values (VEVs). S and ψ are the only two fields in this model which are odd under this residual \mathbb{Z}_2 symmetry. The effect of spontaneous breaking of local gauge symmetry is manifested by the presence of five gauge bosons namely W^\pm , Z , Z' and A , out of which one neutral gauge field (A) remains massless which is identified as the “photon” (mediator of electromagnetic interaction). Thus, in the present scenario we have one extra neutral gauge boson (Z') compared to the SM as we have considered a larger symmetry group here. This neutral gauge boson (Z') is known as the “dark photon” [43] due to its nature of interactions with the electrically charged fermions of the Standard Model. Dark photon plays an important role in this proposed two component dark matter model as it is the main interaction mediator through which both the dark matter candidates interact mutually.

In the present two component dark matter model, the anomalous γ -ray excess is produced by the hadronisation processes of the b quarks, originated only from the self annihilation ($SS^\dagger \rightarrow b\bar{b}$) of the dark matter candidate S at the GC. Therefore as mentioned in Ref. [10], the mass and the $b\bar{b}$ annihilation cross section (actually annihilation cross section times relative velocity) of DM component S need to be in the range 30 GeV–40 GeV and $\sim (1.4\text{--}2.0)\times 10^{-26}$ cm³/s respectively. In order to satisfy the above condition on $\sigma v_{b\bar{b}}$, S must annihilate significantly into $b\bar{b}$ final state which is possible only when $M_S < M_{Z'}$ such that $SS^\dagger \rightarrow Z'Z'$ annihilation mode is kinematically forbidden. On the other hand, since the dark matter component ψ interacts feebly with the SM particles (through tiny mixing between Z and Z'), therefore its dominant interaction channels are $\psi\bar{\psi} \rightarrow Z'Z'$, SS^\dagger . Both of these interaction modes become kinematically inaccessible when $M_\psi < M_{Z'}$, M_S . However for $M_\psi > M_S$ at least one of the interaction channels ($\psi\bar{\psi} \rightarrow SS^\dagger$) is possible. Thus, throughout this present work we have assumed $M_\psi > M_S$ and consequently, the mass (M_ψ) of the dark matter component ψ is taken in the range 60 GeV to 150 GeV. We have found that our computed γ -ray fluxes from the Galactic Centre region for $M_S = 35$ GeV and two different values of M_ψ , namely $M_\psi = 60$ GeV and 80 GeV, can explain the Fermi-LAT data well as long as the quantity called the “effective annihilation cross section” instead of the actual annihilation cross section ($\langle\sigma v_{SS^\dagger \rightarrow b\bar{b}}\rangle$) for the annihilation channel $SS^\dagger \rightarrow b\bar{b}$ lies in the range $(1.52 - 1.67) \times 10^{-26}$ cm³/s. Moreover, the γ -ray fluxes obtained for $M_\psi \geq 100$ GeV become incompatible with the available experimental data. The “effective annihilation cross section” ($\langle\sigma v_{SS^\dagger \rightarrow b\bar{b}}\rangle'$) of the DM component S for the annihilation channel $SS^\dagger \rightarrow b\bar{b}$ is defined as the product of annihilation cross section ($\langle\sigma v_{SS^\dagger \rightarrow b\bar{b}}\rangle$) of the process $SS^\dagger \rightarrow b\bar{b}$ and the square of the fractional contribution of the DM component S to the total relic density.

In our present two component dark matter model the lighter DM component S interacts with the visible sector (SM particles) mainly through the exchange of scalar particles such as Higgs boson h and another neutral scalar boson H ⁴. There exist few single component dark matter models [27, 32] in the literature where the DM candidate also possesses similar type of interactions with the SM particles. These dark matter models are collectively known as the “scalar portal” dark matter model. It is shown in these articles that for the case of low mass dark matter candidate (DM mass $M_{\text{DM}} < M_h/2$ ⁵), the limit on the dark matter relic density from the PLANCK experiment [44], the bounds on spin independent scattering cross section of the DM particle from the direct detection experiments like XENON 100 [45], LUX [46] and the limit on the invisible branching ratio ($h \rightarrow \text{DMDM}$) [47] of the SM Higgs boson are satisfied simultaneously only when the mass of the additional neutral scalar field H is two times the

⁴for definition of H see Eq. (18) of Section 2.

⁵ M_h is the mass of SM Higgs boson h ,

mass of the DM particle. This is very fine tuning situation because there exists no symmetry in the theory which can explain why the dark matter particle mass is exactly half of the mass of the mediator particle. However, in the two component dark matter scenario we do required such type of constraint on the mass of H . We have found that in order to satisfy all the above mentioned experimental and observational bounds, the mass of H has to be in the range $\sim 2M_S$ to $2M_S + \Delta M$, where ΔM is ~ 10 GeV for $M_S = 30$ GeV to 40 GeV (see right panel of Fig. 6 in Section 4).

This paper is organised as follows. In Section 2, we first propose the present two component dark matter model and then study elaborately all the relevant constraints that can be imposed on this proposed model from the theoretical, experimental as well as the observational bounds. Section 3 describes the coupled Boltzmann equations, required for computing the individual relic densities of each dark matter candidate and hence the overall relic density of the dark matter in the Universe. The results that we have obtained by solving the coupled Boltzmann equations numerically and using various experimental, observational and theoretical constraints are discussed in Section 4. In Section 5 we calculate the γ -ray flux for this proposed two component dark matter scenario and is compared with the available Fermi-LAT data. We have also compared the range of allowed values of “effective annihilation cross section” of S for $b\bar{b}$ annihilation channel with the limits reported by the Fermi-LAT and DES collaborations from their analyses using data obtained from various dwarf spheroidal galaxies. Finally, in Section 6 we summarise our work.

2 The Model

We propose a two component dark matter model where the dark sector is composed of a complex scalar (S) and a Dirac fermion (ψ), both of which are singlets under the Standard Model gauge group $SU(3)_c \times SU(2)_L \times U(1)_Y$. Thus, in the scalar sector of the model we have the usual Higgs doublet Φ and two complex SM gauge singlets S, Φ_s . Note that the present model is an extension of the Standard Model of particle physics in all three sectors namely, gauge, fermionic as well as scalar sector. The gauge symmetry group of the SM is enhanced by an additional local $U(1)_X$ symmetry under which all particles except the SM particles (including the Higgs doublet Φ) transform nontrivially. Among the three complex scalars (Φ, Φ_s, S) present in this model only two, namely Φ and Φ_s acquire VEVs. Consequently, the local gauge symmetry $SU(2)_L \times U(1)_Y \times U(1)_X$ is spontaneously broken which gives rise to one extra massive neutral gauge boson Z' in addition to four SM gauge bosons namely W^\pm, Z, A . After the spontaneous

breaking of local $SU(2)_L \times U(1)_Y \times U(1)_X$ symmetry the Lagrangian of this model is left with a residual $U(1)_{\text{em}} \times \mathbb{Z}_2$ symmetry under which only the dark sector particle S and ψ are odd. Now if we consider a renormalisable Lagrangian (terms upto mass dimension four), the field ψ becomes automatically stable as it is the only fermionic field which transforms nontrivially under $U(1)_X$. However, by choosing proper $U(1)_X$ charges (Q_X) among the dark sector particles (ψ , S) and Φ_s , ψ can be made stable for the terms whose mass dimension exceed four. This requires $Q_X(\psi) \neq Q_X(S)$ such that the stability violating terms of ψ (decay terms) arising from the higher dimensional effective operators (suppressed by some high energy scale Λ) are either totally forbidden from symmetry argument or suppressed by higher powers of Λ . The assigned gauge charges and VEVs of all the fields present in this model are given below in a tabular form (see Table 1). Moreover, the other dark sector particle S becomes stable by application of the residual \mathbb{Z}_2 symmetry.

Field	SU(2)_L charge	U(1)_Y charge	U(1)_X charge	VEV
Φ	2	$\frac{1}{2}$	0	v
Φ_s	1	0	$\frac{1}{2}$	v_s
S	1	0	2	0
ψ	1	0	1	0
l_L	2	$-\frac{1}{2}$	0	0
Q_L	2	$\frac{1}{6}$	0	0
e_R	1	-1	0	0
u_R	1	$\frac{2}{3}$	0	0
d_R	1	$-\frac{1}{3}$	0	0

Table 1: $SU(2)_L \times U(1)_Y \times U(1)_X$ charges and VEVs of all fields (including SM fermions) involved in the present model, where l_L , Q_L are left handed lepton and quark doublet while e_R , u_R and d_R represent right handed charge lepton, up type and down type quark respectively.

The Lagrangian of the present model is then given by,

$$\mathcal{L} \supset \mathcal{L}_{\text{gauge}} + \mathcal{L}_{\text{fermion}} + \mathcal{L}_{\text{scalar}} , \quad (1)$$

where $\mathcal{L}_{\text{gauge}}$ is the Lagrangian of the gauge fields corresponding to the gauge group $U(1)_Y$ and $U(1)_X$.

$$\mathcal{L}_{\text{gauge}} = -\frac{1}{4}\hat{B}_{\mu\nu}\hat{B}^{\mu\nu} - \frac{1}{4}\hat{X}_{\mu\nu}\hat{X}^{\mu\nu} + \frac{\chi}{2}\hat{X}_{\mu\nu}\hat{B}^{\mu\nu} , \quad (2)$$

with

$$\hat{B}_{\mu\nu} = \partial_\mu \hat{B}_\nu - \partial_\nu \hat{B}_\mu \quad \text{and} \quad \hat{X}_{\mu\nu} = \partial_\mu \hat{X}_\nu - \partial_\nu \hat{X}_\mu. \quad (3)$$

In the above Eq. (3) B_μ and X_μ represent gauge fields corresponding to the unitary gauge groups $U(1)_Y$ and $U(1)_X$ respectively. Hat notations on the gauge fields indicate that kinetic terms of B_μ and X_μ are not diagonal. The coefficient of kinetic mixing term between the two $U(1)$ gauge fields in Eq. (2) is denoted by $\chi = \frac{\epsilon}{\cos\theta_W}$ which is experimentally constrained to be very small. Consider a $GL(2, R)$ rotation from the basis $\hat{B}_\mu, \hat{X}_\mu \rightarrow B_\mu, X_\mu$ in such a way that with respect to new basis kinetic mixing term vanishes.

$$\begin{pmatrix} B_\mu \\ X_\mu \end{pmatrix} = \begin{pmatrix} 1 & -\chi \\ 0 & \sqrt{1-\chi^2} \end{pmatrix} \begin{pmatrix} \hat{B}_\mu \\ \hat{X}_\mu \end{pmatrix}. \quad (4)$$

After such rotation,

$$\hat{B}_\mu \simeq B_\mu + \chi X_\mu \quad \text{and} \quad \hat{X}_\mu \simeq X_\mu. \quad (5)$$

Since $\chi \ll 1$ [43, 48, 49], we have ignored $\mathcal{O}(\chi^2)$ terms in the above equation (Eq. (5)). Spontaneous breaking of $SU(2)_L \times U(1)_Y \times U(1)_X$ symmetry by VEVs of the neutral components of the scalar doublet Φ (CP even part) and the complex singlet scalar Φ_s respectively (see Table. 1), results in a 3×3 mass square mixing matrix between the three neutral gauge bosons namely $W_{3\mu}, B_\mu, X_\mu$.

$$\mathcal{M}_{\text{gauge}}^2 = \frac{v^2}{4} \begin{pmatrix} g^2 & -gg' & -\chi gg' \\ -gg' & g'^2 & \chi g'^2 \\ -\chi gg' & \chi g'^2 & g_X^2 \left(\frac{v_s}{v}\right)^2 \end{pmatrix}. \quad (6)$$

After diagonalising this mass square mixing matrix by an orthogonal matrix $O(\theta_{\text{NB}}, \theta_W)$ we obtain three physical neutral gauge fields which are denoted by Z_μ, A_μ and Z'_μ . The eigenstates of the matrix $\mathcal{M}_{\text{gauge}}^2$ namely, Z_μ, A_μ and Z'_μ are linearly related to $W_{3\mu}, B_\mu, X_\mu$ by an orthogonal transformation which is given by,

$$\begin{pmatrix} Z_\mu \\ A_\mu \\ Z'_\mu \end{pmatrix} = O(\theta_{\text{NB}}, \theta_W) \begin{pmatrix} W_{3\mu} \\ B_\mu \\ X_\mu \end{pmatrix}, \quad (7)$$

with

$$O(\theta_{\text{NB}}, \theta_W) = \begin{pmatrix} \cos\theta_{\text{NB}} \cos\theta_W & -\cos\theta_{\text{NB}} \sin\theta_W & -\sin\theta_{\text{NB}} \\ \sin\theta_W & \cos\theta_W & 0 \\ \sin\theta_{\text{NB}} \cos\theta_W & -\sin\theta_{\text{NB}} \sin\theta_W & \cos\theta_{\text{NB}} \end{pmatrix}, \quad (8)$$

where θ_W and θ_{NB} are the usual weak mixing angle and the mixing angle between two neutral gauge bosons Z and Z' respectively. The expressions of θ_W and θ_{NB} are given by,

$$\theta_W = \tan^{-1} \left(\frac{g'}{g} \right) , \quad \theta_{NB} = \frac{1}{2} \tan^{-1} \left(\frac{2\epsilon \tan \theta_W}{1 - \frac{g_X^2 v_s^2}{g^2 + g'^2}} \right) . \quad (9)$$

Among the three physical neutral gauge bosons one remains massless which is identified as the ‘photon’. The masses of other two neutral bosons namely Z and Z' are given by,

$$\begin{aligned} M_Z &= \sqrt{\frac{g_Z^2 v^2 + g_X^2 v_s^2}{8} + \frac{1}{8} \sqrt{(g_Z^2 v^2 - g_X^2 v_s^2)^2 + 4(g' g_Z v^2 \chi)^2}} , \\ M_{Z'} &= \sqrt{\frac{g_Z^2 v^2 + g_X^2 v_s^2}{8} - \frac{1}{8} \sqrt{(g_Z^2 v^2 - g_X^2 v_s^2)^2 + 4(g' g_Z v^2 \chi)^2}} , \end{aligned} \quad (10)$$

where

$$g_Z = \sqrt{g^2 + g'^2} ,$$

using the condition $\chi \ll 1$ as mentioned before, Eq. (10) reduces to

$$\begin{aligned} M_Z^2 &\simeq \frac{g_Z^2 v^2}{4} , \\ M_{Z'}^2 &\simeq \frac{g_X^2 v_s^2}{4} . \end{aligned} \quad (11)$$

In Eq. (1), $\mathcal{L}_{\text{fermion}}$ refers to the Lagrangian of the singlet Dirac fermion ψ , which is given by,

$$\mathcal{L}_{\text{fermion}} = \bar{\psi} (i \mathcal{D}_\psi - M_\psi) \psi , \quad (12)$$

where the covariant derivative \mathcal{D}_ψ of the field ψ is defined as,

$$\begin{aligned} \mathcal{D}_\psi \psi &= \gamma^\mu D_\mu \psi , \\ &= \gamma^\mu (\partial_\mu + i g_X X_\mu) \psi . \end{aligned} \quad (13)$$

The scalar sector Lagrangian $\mathcal{L}_{\text{scalar}}$ (in Eq. (1)) of the present model has the following form

$$\begin{aligned} \mathcal{L}_{\text{scalar}} &= (D_{\phi_\mu} \Phi)^\dagger (D_{\phi^\mu} \Phi) + (D_{\phi_{s\mu}} \Phi_s)^\dagger (D_{\phi_s^\mu} \Phi_s) + (D_{s\mu} S)^\dagger (D_s^\mu S) \\ &\quad - V(\Phi, \Phi_s, S) , \end{aligned} \quad (14)$$

with

$$\begin{aligned} V(\Phi, \Phi_s, S) &= \mu^2 (\Phi^\dagger \Phi) + \lambda (\Phi^\dagger \Phi)^2 + \mu_s^2 (\Phi_s^\dagger \Phi_s) + \lambda_s (\Phi_s^\dagger \Phi_s)^2 + \rho^2 (S^\dagger S) \\ &\quad + \kappa (S^\dagger S)^2 + \lambda_1 (\Phi^\dagger \Phi) (\Phi_s^\dagger \Phi_s) + \lambda_2 (\Phi^\dagger \Phi) (S^\dagger S) \\ &\quad + \lambda_3 (\Phi_s^\dagger \Phi_s) (S^\dagger S) , \end{aligned} \quad (15)$$

where

$$\begin{aligned}
D_{\phi_\mu}\Phi &= \left(\partial_\mu + i\frac{g}{2}\sigma^a W_{a\mu} + i\frac{g'}{2}(B_\mu + \chi X_\mu) \right) \Phi, \\
D_{\phi_{s\mu}}\Phi_s &= \left(\partial_\mu + i\frac{g_X}{2}X_\mu \right) \Phi_s, \\
D_{s\mu}S &= (\partial_\mu + i2g_X X_\mu) S,
\end{aligned} \tag{16}$$

are the covariant derivatives of the scalar doublet Φ and two complex scalar singlets Φ_s , S respectively. Similar to the gauge sector, the scalar sector also exhibits mixing between two real scalars namely ϕ^0 (neutral CP even part of the doublet Φ) and ϕ_s^0 (real part of the complex scalar Φ_s) after spontaneous breaking of gauge symmetry $(\text{SU}(2)_L \times \text{U}(1)_Y \times \text{U}(1)_X)$. The mass square mixing matrix between these two real scalars are given by,

$$\mathcal{M}_{\text{scalar}}^2 = \begin{pmatrix} 2\lambda v^2 & \lambda_1 v_s v \\ \lambda_1 v_s v & 2\lambda_s v_s^2 \end{pmatrix}. \tag{17}$$

Diagonalising $\mathcal{M}_{\text{scalar}}^2$ by an orthogonal matrix $O(\alpha)$, we obtain two real physical scalars namely h and H . The old basis states (ϕ^0, ϕ_s^0) and the eigenstates (h, H) of the matrix $\mathcal{M}_{\text{scalar}}^2$ are linearly related by the orthogonal matrix $O(\alpha)$ which is given by,

$$\begin{pmatrix} h \\ H \end{pmatrix} = \begin{pmatrix} \cos \alpha & -\sin \alpha \\ \sin \alpha & \cos \alpha \end{pmatrix} \begin{pmatrix} \phi^0 \\ \phi_s^0 \end{pmatrix}. \tag{18}$$

The mixing angle α and the masses of the physical real scalars h and H are

$$\alpha = \frac{1}{2} \tan^{-1} \left(\frac{\frac{\lambda_1 v}{\lambda_s v_s}}{1 - \frac{\lambda v^2}{\lambda_s v_s^2}} \right), \tag{19}$$

$$\begin{aligned}
M_h &= \sqrt{\lambda v^2 + \lambda_s v_s^2 + \sqrt{(\lambda v^2 - \lambda_s v_s^2)^2 + (\lambda_1 v v_s)^2}}, \\
M_H &= \sqrt{\lambda v^2 + \lambda_s v_s^2 - \sqrt{(\lambda v^2 - \lambda_s v_s^2)^2 + (\lambda_1 v v_s)^2}}.
\end{aligned} \tag{20}$$

Between these two real scalars, h plays the role of SM Higgs boson. The mass term of the scalar field S which does not mix with other components of the scalar sector is given by,

$$M_S = \sqrt{\rho^2 + \frac{\lambda_2 v^2}{2} + \frac{\lambda_3 v_s^2}{2}}. \tag{21}$$

Both the fermionic field ψ and complex scalar field S remain decoupled from the visible sector of the model. Thus, they can be viable components of dark matter. From the above discussion

it is evident that the present scenario involves 10 unknown parameters namely, masses of two dark matter components namely M_S and M_ψ , mass of one neutral scalar (M_H)⁶, mass of extra neutral gauge boson ($M_{Z'}$), the gauge coupling g_X corresponding to the gauge group $U(1)_X$, neutral scalars mixing angle (α), coefficient of kinetic mixing term (ϵ), quartic self coupling (κ)⁷ of S and other two quartic couplings λ_2, λ_3 of Φ between S and Φ_s respectively. The allowed ranges of these parameters will be restricted by imposing both experimental, observational as well as theoretical bounds mentioned below.

- **Vacuum Stability** - In order to obtain a stable vacuum, the scalar potential $V(\Phi, \Phi_s, S)$ (Eq. (15)) of the present model must be bounded from below. This will be maintained if the following conditions are satisfied,

$$\begin{aligned}
\lambda &\geq 0, \lambda_s \geq 0, \kappa \geq 0, \\
\lambda_1 &\geq -2\sqrt{\lambda \lambda_s}, \\
\lambda_2 &\geq -2\sqrt{\lambda \kappa}, \\
\lambda_3 &\geq -2\sqrt{\lambda_s \kappa}, \\
\sqrt{\lambda_1 + 2\sqrt{\lambda \lambda_s}} \sqrt{\lambda_2 + 2\sqrt{\lambda \kappa}} \sqrt{\lambda_3 + 2\sqrt{\lambda_s \kappa}} \\
&+ 2\sqrt{\lambda \lambda_s \kappa} + \lambda_1 \sqrt{\kappa} + \lambda_2 \sqrt{\lambda_s} + \lambda_3 \sqrt{\lambda} \geq 0 \quad .
\end{aligned} \tag{22}$$

- **Zero VEV of S** - In the present scenario we assume that one among the three scalars, namely S does not possess any vacuum expectation value. The VEV of other two scalars are v and v_s respectively (see Table 1). Hence the ground state of the model is $(v, v_s, 0)$ which requires

$$\mu^2 < 0, \quad \mu_s^2 < 0 \quad \text{and} \quad \rho^2 > 0 \quad . \tag{23}$$

- **PLANCK Limit** - The total relic density ($\Omega_T h^2$) of the dark matter components must lie within the range [44] specified by the PLANCK experiment. The PLANCK limit for the relic density of the dark matter in the Universe is

$$0.1172 < \Omega_{\text{DM}} h^2 < 0.1226 \quad \text{at} \quad 68\% \quad \text{C.L.} \tag{24}$$

- **Limits from Dark Matter Direct Detection Experiments** - In our two component dark matter model both the dark matter components namely S and ψ can interact with

⁶as we identify one of the neutral scalars namely h with the SM Higgs boson, therefore its mass is fixed at ~ 125.5 GeV [50, 51].

⁷Through out this work we have kept κ fixed at 0.1

detector nuclei placed at various underground laboratories. The component ψ scatters off the detector nuclei only via exchange of Z and Z' bosons, while for the other component S , the dominant contribution comes mainly through the exchange of scalar particles such as SM like Higgs boson (h) and H . Fig. 1 shows the Feynman diagrams for the scattering of both the dark matter components with the detector nucleon (N). The spin independent

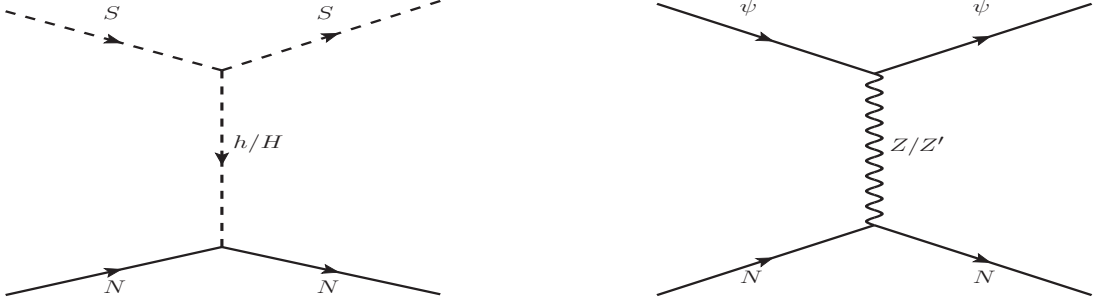


Figure 1: Feynman diagrams for the elastic scattering between both the dark matter candidates S , ψ and the nucleon N of the detector material.

scattering cross section between the dark matter component ψ and nucleon N is given by [52],

$$\sigma_{\text{SI}}^{\psi N \rightarrow \psi N} \simeq \frac{\sqrt{2} G_{\text{F}} M_Z^2 g_X^2 Q_X(\psi)^2 \sin^2 \theta_{\text{NB}} \cos^2 \theta_{\text{NB}} \mu_{\psi N}^2 F_1^z}{16\pi} \left(\frac{1}{M_Z^2} - \frac{1}{M_{Z'}^2} \right)^2, \quad (25)$$

where

$$\mu_{\psi N} = \frac{M_\psi M_N}{(M_\psi + M_N)}$$

is the reduced mass between ψ and N , $F_1^z = -0.5$ is the form factor for neutron and $Q_X(\psi) = 1$ is the $U(1)_X$ charge of ψ . The expression of spin independent scattering cross section for the process $SN \rightarrow SN$ is given by,

$$\sigma_{\text{SI}}^{SN \rightarrow SN} \simeq \frac{\mu_{SN}^2}{4\pi} \left(\frac{M_N f}{M_S v} \right)^2 \left(\frac{g_{SSh} \cos \alpha}{M_h^2} + \frac{g_{SSH} \sin \alpha}{M_H^2} \right)^2, \quad (26)$$

with

$$\mu_{SN} = \frac{M_S M_N}{(M_S + M_N)},$$

where

$$\begin{aligned} g_{SSh} &= -(\lambda_2 v \cos \alpha - \lambda_3 v_s \sin \alpha), \\ g_{SSH} &= -(\lambda_2 v \sin \alpha + \lambda_3 v_s \cos \alpha) \end{aligned} \quad (27)$$

are the couplings for the vertex SSh and SSH respectively. f is the relevant form factor. Throughout this work, we have adopted the value of $f = 0.3$ [53–55].

The Dark sector in our model is composed of two kinds of particles, one of which is scalar (however, it has different antiparticle⁸ (complex scalar)) while the other component is fermionic (Dirac fermion) in nature. Their masses as well as the contributions to the total relic density of the dark matter are different in general. Consequently the number densities n_S, n_ψ for these two components at the present epoch are also different. Therefore when we compare the spin independent scattering cross sections computed for both the dark matter components (S and ψ) within the framework of the present two component DM model with the available experimental data (exclusion plots from various ongoing dark matter direct detection experiments such as LUX [46], XENON-100 [45] etc.), one has to keep in mind that the exclusion plots are computed with the assumption that all the dark matter present in the Universe are same in nature *i.e.* interaction rates with the detector nuclei are same for all the dark matter particles. However, this assumption is certainly not true in our case as we have two component dark matter scenario. Hence we need to rescale both $\sigma_{\text{SI}}^{\psi N \rightarrow \psi N}$ and $\sigma_{\text{SI}}^{SN \rightarrow SN}$ (Eqs. (25)-(26)) by appropriate factors consistent with the present consideration that we have two types of dark matter in the Universe. We define the spin independent “effective scattering cross section” between the detector nucleon N and the dark matter component i as,

$$\sigma'_{\text{SI}}{}^{iN \rightarrow iN} = \frac{n_i}{n_i + n_j} \sigma_{\text{SI}}{}^{iN \rightarrow iN}, \quad (28)$$

with $i, j = S, \psi$ and $i \neq j$, n_i is the number density of the dark matter component i at the present epoch. For a viable two component dark matter model it is desirable that

$$\sigma'_{\text{SI}}{}^{iN \rightarrow iN} < \sigma_{\text{SI}}^{\text{Exp}}(M_i). \quad (29)$$

In the above M_i is the mass of the i^{th} type dark matter and $\sigma_{\text{SI}}^{\text{Exp}}(M_i)$ is the experimental upper bound for the spin independent scattering cross section between dark matter particle of mass M_i and the nucleon N . In this work we have used results only from LUX experiment for constraining the relevant parameter space of this model since LUX imposes strongest limits (exclusion plot) in $\sigma_{\text{SI}} - M_{\text{DM}}$ plane until now.

- **Precision electroweak observable** - We have already shown earlier, in this section, that the dark photon Z' possesses a nonzero mixing with the SM gauge boson Z due to the presence of a kinetic mixing term in the Lagrangian (Eq. (2)) between the hypercharge

⁸particle and antiparticle possess different $U(1)_X$ charges.

gauge boson \hat{B}_μ and the $U(1)_X$ gauge boson \hat{X}_μ . As a result of this nonzero $Z - Z'$ mixing, the values of electroweak precision observables, namely the mass (M_Z) and the decay width (Γ_Z) of Z boson, the rho parameter (ρ) as well as the electroweak oblique parameters (S , T , U parameters or Peskin Takeuchi parameters [56]), get shifted from their SM predictions. Therefore, the experimentally measured values of these parameters constrain the allowed ranges of kinetic mixing parameter ϵ and the mixing angle θ_{NB} . Thus while computing the allowed range for the $Z - Z'$ mixing angle θ_{NB} we have considered the following constraints,

- The deviation of the physical Z boson mass from its SM value should remain within the range given by [57], [58]

$$\frac{M_Z - M_{Z_0}}{M_{Z_0}} \leq 2.4 \times 10^{-5} , \quad (30)$$

where M_{Z_0} is the mass of Z boson predicted from the SM of particle physics.

- The nonzero mixing angle θ_{NB} between Z and Z' allows the physical Z boson to decay into the final state comprised of particle and anti-particle of dark matter candidate S . This additional decay mode is known as the non-Standard invisible decay channel of Z ⁹. Therefore, the total decay width of Z boson is

$$\Gamma_Z^{\text{tot}} = \sum_f \Gamma_{Z \rightarrow f\bar{f}} + \Gamma_{Z \rightarrow S S^\dagger} , \quad (31)$$

where f is any SM model fermion except t quark. In order to satisfy the precisely measured decay width of Z boson, $\Gamma_Z = 2.4952 \pm 0.0023$ GeV [57], as reported by the LEP [59], the non-Standard invisible decay width ($\Gamma_{Z \rightarrow S S^\dagger}$) of Z boson should obey the following limit

$$\Gamma_{Z \rightarrow S S^\dagger} \leq 2.3 \text{ MeV} . \quad (32)$$

The expressions of $\Gamma_{Z \rightarrow f\bar{f}}$ and $\Gamma_{Z \rightarrow S S^\dagger}$ are given by

$$\Gamma_{Z \rightarrow f\bar{f}} = \frac{n_c g^2 M_Z}{48\pi \cos^2 \theta_W} (a_f^2 + b_f^2) \left(1 + \frac{2(a_f^2 - 2b_f^2) M_f^2}{(a_f^2 + b_f^2) M_Z^2} \right) \sqrt{1 - \frac{4M_f^2}{M_Z^2}} , \quad (33)$$

$$\Gamma_{Z \rightarrow S S^\dagger} = \frac{g_X^2 Q_X(S)^2 \sin^2 \theta_{\text{NB}} M_Z}{48\pi} \left(1 - \frac{4M_S^2}{M_Z^2} \right)^{3/2} , \quad (34)$$

⁹In this present model SM Z boson can also decay into a final state containing ψ and $\bar{\psi}$ through its nonzero mixing with Z' . This decay channel is also another non-standard decay mode of the SM Z boson. However, this decay mode is kinematically forbidden for the entire adopted range of M_ψ .

with

$$a_f = t_3 a - 2Q_f(a - \cos\theta_{\text{NB}} \cos^2\theta_{\text{W}}) , \quad (35)$$

$$b_f = t_3 a , \quad (36)$$

and

$$a = \cos\theta_{\text{NB}} + \epsilon \tan\theta_{\text{W}} \sin\theta_{\text{NB}} . \quad (37)$$

In the above Eq. (34) M_f , Q_f and t_3 are the mass, electrical charge and isospin quantum number of the SM fermion f while $Q_X(S) = 2$ is the $U(1)_X$ charge of the dark matter particle S (Table 1) while $n_c = 1$ (3) is the colour charge of the SM lepton (quark).

- $Z - Z'$ mixing shifts the value of the tree level ρ parameter from its Standard Model value which is equal to one. For small value of mixing angle (θ_{NB}) between Z and Z' the deviation of ρ parameter from its SM value is given by [60]

$$\Delta\rho \simeq \epsilon \tan\theta_{\text{W}} \frac{M_{Z_0}^2}{M_Z^2} \theta_{\text{NB}} . \quad (38)$$

Thus, in order to keep the value of ρ parameter within the range as specified in Refs. [57, 59], the allowed ranges of ϵ as well as θ_{NB} will be constrained.

- There will be some extra contributions to the Electroweak oblique parameters [56], mainly in S and T parameter, which result in from the nonzero mixing between the SM gauge boson Z and dark gauge boson Z' . The $Z - Z'$ contributions to the S and T parameters for the lowest order in θ_{NB} are given in Ref. [61]. We have varied the relevant parameters, namely ϵ , $M_{Z'}$, in such a way that the electroweak oblique parameters always lie within the range as given in Refs. [62]

$$S = 0.05 \pm 0.11 , \quad T = 0.09 \pm 0.13 , \quad U = 0.01 \pm 0.11. \quad (39)$$

• Constraint from LHC results

- **Dilepton Production-** Moreover, there exists strong upper bound on the mixing angle θ_{NB} between Z and Z' from ATLAS [63] and CMS [64] collaborations for the processes like $pp \rightarrow Z'X \rightarrow f\bar{f}X$ ($f = e, \mu$) since the fermiophobic Z' couples to the SM leptons only through the mixing angle θ_{NB} . In Ref. [65] the upper limits on the kinetic mixing parameter χ ($\equiv \frac{\epsilon}{\cos\theta_{\text{W}}}$) are given with the mass of Z' varies in the range $166 \text{ GeV} \lesssim M_{Z'} \lesssim 3 \text{ TeV}$. These limits are obtained from the upper bounds on “signal

cross section times branching fraction” σBR for the above mentioned processes as reported by the ATLAS collaboration [63]. For lighter Z' , which we are considering in this work, the upper bounds on χ , obtained from electroweak precision data (EWPD) constraints [58], are also given in Ref. [65]. From the Fig. 6 of Ref. [65] it is evident that the upper bound on kinetic mixing parameter χ , using EWPD as constraints, varies from $\sim 10^{-1.55}$ to $\sim 10^{-1.83}$ for $10 \text{ GeV} \leq M_{Z'} \leq 80 \text{ GeV}$. The corresponding upper bound on the mixing angle θ_{NB} (computed using Eq. (9)) varies in the range $\sim 0.01 \text{ rad}$ to $\sim 0.03 \text{ rad}$.

- **Signal strength of the SM like Higgs boson h** - The signal strength ratio of Higgs boson for a particular decay channel ($h \rightarrow X\bar{X}$) is given by,

$$R_{X\bar{X}} = \frac{\sigma}{\sigma_{\text{SM}}} \frac{\text{BR}(h \rightarrow X\bar{X})}{\text{BR}(h \rightarrow X\bar{X})^{\text{SM}}}, \quad (40)$$

where X is any SM fermion / gauge boson. In Eq. (40) σ and $\text{BR}(h \rightarrow X\bar{X})$ are the Higgs production cross section and the branching ratio of the decay channel $h \rightarrow X\bar{X}$ for this present model respectively. Similar quantities for the SM are denoted by σ_{SM} and $\text{BR}(h \rightarrow X\bar{X})^{\text{SM}}$ respectively. In order to satisfy LHC results [66] we take $R_{X\bar{X}} \geq 0.8$ for any SM particle X .

- **Invisible decay width of Higgs boson (Γ_{inv})** - In this present two component dark matter model, the SM like Higgs boson h can decay into final states that consist of S, S^\dagger , if the kinematical condition $M_h > 2M_S$ is satisfied. Moreover if $M_h > 2M_H$, h can also decay into a pair of H which subsequently decays into S and S^\dagger . Therefore, the actual invisible decay width of the SM like Higgs boson h is given by

$$\Gamma_h^{\text{inv}} = \Gamma_{h \rightarrow SS^\dagger} + \Gamma_{h \rightarrow HH} \times (\text{BR}(H \rightarrow SS^\dagger))^2, \quad (41)$$

with

$$\Gamma_{h \rightarrow SS^\dagger} = \frac{g_{SSh}^2}{16\pi M_h} \sqrt{1 - \frac{4M_S^2}{M_h^2}}, \quad (42)$$

$$\Gamma_{h \rightarrow HH} = \frac{g_{HHh}^2}{8\pi M_h} \sqrt{1 - \frac{4M_H^2}{M_h^2}} \quad (43)$$

and

$$g_{HHh} = -\frac{\lambda_1}{2} \left(v \cos^3 \alpha - v_s \sin^3 \alpha - 2v_s \cos^2 \alpha \sin \alpha - 2v \sin^2 \alpha \cos \alpha \right) + 3\lambda_s v_s \cos^2 \alpha \sin \alpha - 3\lambda v \cos \alpha \sin^2 \alpha, \quad (44)$$

is the coupling strength for the vertex involving two H and one h while $\text{BR}(H \rightarrow SS^\dagger)$ is the branching fraction of H decaying into SS^\dagger final state. Throughout the work, we assume that the total invisible branching ratio (BR_{inv}) of the SM like Higgs boson (h) is less than 20% [47] of its total decay width (Γ_h).

3 Solution of Coupled Boltzmann Equations of two Dark Matter Components ψ and S

In the present model, the dark sector has two different types of particles namely, a Dirac fermion ψ and a complex scalar S . Therefore, the total relic density of the dark matter in the Universe must have contributions from both of these dark sector particles. In order to compute the total relic density as well as individual relic densities of each dark matter candidate, it is essential to solve two coupled Boltzmann equations [40,67] which describe the evolution of number densities of both the dark matter candidates. The equations are given by,

$$\frac{dn_\psi}{dt} + 3n_\psi H = -\langle\sigma v_{\psi\bar{\psi}\rightarrow X\bar{X}}\rangle (n_\psi^2 - (n_\psi^{\text{eq}})^2) - \langle\sigma v_{\psi\bar{\psi}\rightarrow SS^\dagger}\rangle \left(n_\psi^2 - \frac{(n_\psi^{\text{eq}})^2}{(n_S^{\text{eq}})^2} n_S^2 \right), \quad (45)$$

$$\frac{dn_S}{dt} + 3n_S H = -\langle\sigma v_{SS^\dagger\rightarrow X\bar{X}}\rangle (n_S^2 - (n_S^{\text{eq}})^2) + \langle\sigma v_{\psi\bar{\psi}\rightarrow SS^\dagger}\rangle \left(n_\psi^2 - \frac{(n_\psi^{\text{eq}})^2}{(n_S^{\text{eq}})^2} n_S^2 \right), \quad (46)$$

where n_ψ , n_S denote the number densities of ψ and S while their equilibrium values are denoted by n_ψ^{eq} , n_S^{eq} respectively, H is the Hubble's constant. $\sigma v_{SS^\dagger\rightarrow X\bar{X}}$ describes the self annihilation cross section of the dark matter component S into the SM particles as well as other non SM particles such as Z' , H^{10} while the same quantity for the other DM component (ψ) is denoted by $\sigma v_{\psi\bar{\psi}\rightarrow X\bar{X}}$ ¹¹. The interaction between the two components of dark matter is described by the annihilation cross section $\sigma v_{\psi\bar{\psi}\rightarrow SS^\dagger}$ where the heavier dark matter component (say ψ) annihilates to produce other component S . New gauge boson Z' is the main exchange particle for this interaction. The Feynman diagrams for all the processes (self annihilations of both the dark matter components and dark matter conversion from heavier to lighter) which are relevant for the evolution of number densities of S and ψ are given in Fig. 2. The annihilation cross sections

¹⁰ X represents any particle in the present model, except ψ , satisfying the kinematic condition $s > 4M_X^2$. Where s being the centre of mass energy and M_X is the mass of X . We will see later that the annihilation channel $SS^\dagger \rightarrow HH$ is kinematically not possible within the allowed ranges of M_H for a particular value of M_S (right panel of Fig. 6).

¹¹For the DM component ψ , $X \neq h, H$ as the Lagrangian of the present model does not contain any of these vertices namely Zhh , $Z'hh$, ZHH and $Z'HH$.

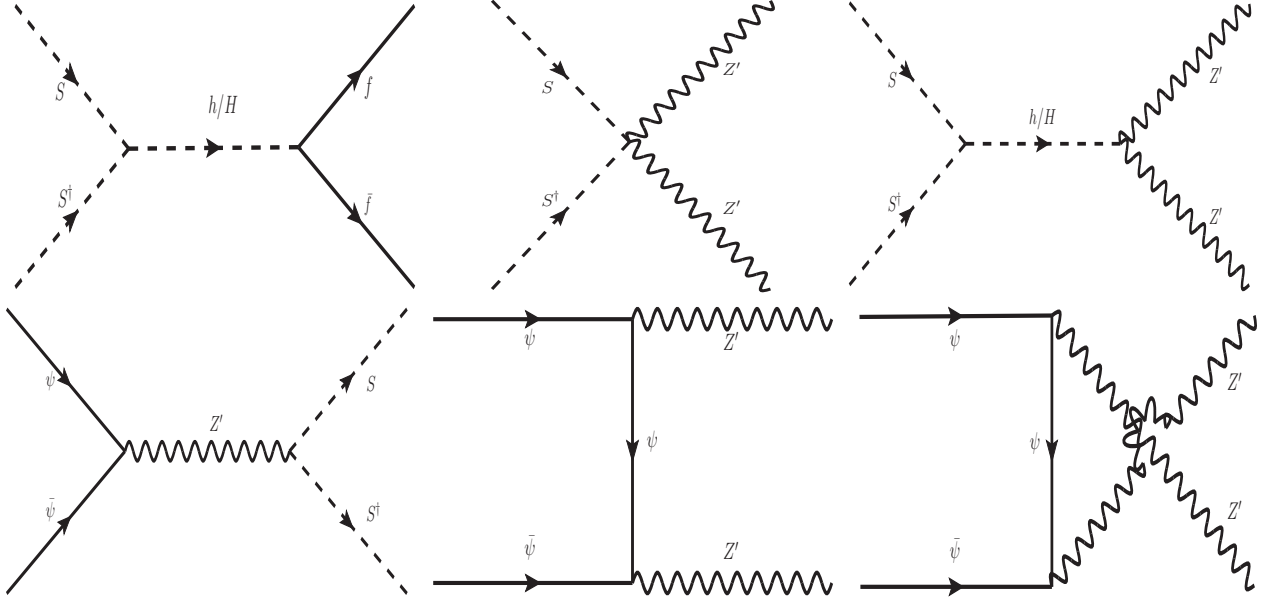


Figure 2: Feynman diagrams for the dominant self annihilation processes of both the dark matter components S , ψ .

for the processes shown in Fig. 2 are given by,

$$\begin{aligned}
\sigma_{\psi\bar{\psi}\rightarrow Z'Z'} &= \frac{(Q_X(\psi) g_X \cos \theta_{\text{NB}})^4}{8\pi s(s - 4M_\psi^2)} \left[-\frac{s\sqrt{1 - \frac{4M_\psi^2}{s}}\sqrt{1 - \frac{4M_{Z'}^2}{s}}(sM_\psi^2 + 4M_\psi^4 + 2M_{Z'}^4)}{M_\psi^2(s - 4M_{Z'}^2) + M_{Z'}^4} + \right. \\
&\quad \left. \frac{(4M_\psi^2(s - 2M_{Z'}^2) - 8M_\psi^4 + 4M_{Z'}^4 + s^2)}{s - 2M_{Z'}^2} \ln \frac{2M_{Z'}^2 - s \left(1 + \sqrt{\left(1 - \frac{4M_\psi^2}{s}\right)\left(1 - \frac{4M_{Z'}^2}{s}\right)}\right)}{2M_{Z'}^2 - s \left(1 - \sqrt{\left(1 - \frac{4M_\psi^2}{s}\right)\left(1 - \frac{4M_{Z'}^2}{s}\right)}\right)} \right], \quad (47)
\end{aligned}$$

$$\begin{aligned}
\sigma_{SS^\dagger\rightarrow f\bar{f}} &= n_c \frac{m_f^2}{8\pi s} (s - 4m_f^2) \sqrt{\frac{s - 4m_f^2}{s - 4M_S^2}} \left[\frac{(g_{SSh})^2 \cos^2 \alpha}{(s - M_h^2)^2 + (\Gamma_h M_h)^2} + \frac{(g_{SSH})^2 \sin^2 \alpha}{(s - M_H^2)^2 + (\Gamma_H M_H)^2} \right. \\
&\quad \left. + \frac{(g_{SSh} g_{SSH}) \sin 2\alpha \{(s - M_h^2)(s - M_H^2) + \Gamma_h \Gamma_H M_h M_H\}}{\{(s - M_h^2)^2 + (\Gamma_h M_h)^2\} \{(s - M_H^2)^2 + (\Gamma_H M_H)^2\}} \right], \quad (48)
\end{aligned}$$

$$\sigma_{SS^\dagger\rightarrow Z'Z'} = \frac{1}{16\pi s} \sqrt{\frac{s - 4M_{Z'}^2}{s - 4M_\psi^2}} \left(|\mathbf{g}|^2 \frac{s^2}{M_{Z'}^4} \right) \left(1 - \frac{4M_{Z'}^2}{s} + \frac{12M_{Z'}^4}{s^4} \right), \quad (49)$$

where

$$\mathfrak{g} = g_X Q_X(S) \cos \theta_{\text{NB}} - \frac{g_{SSH} g_{HZ'Z'} [(s - M_H^2) - i\Gamma_H M_H]}{(s - M_H^2)^2 + (\Gamma_H M_H)^2} - \frac{g_{SSh} g_{hZ'Z'} [(s - M_h^2) - i\Gamma_h M_h]}{(s - M_h^2)^2 + (\Gamma_h M_h)^2}, \quad (50)$$

with

$$g_{hZ'Z'} = \frac{g_Z^2 v}{4} \left\{ b^2 \cos \alpha - \left(\frac{g_X Q_X(\Phi_s)}{g_Z Q_Y(\Phi)} \right)^2 \frac{v_s}{v} \sin \alpha \cos^2 \theta_{\text{NB}} \right\},$$

$$g_{HZ'Z'} = \frac{g_Z^2 v}{4} \left\{ b^2 \sin \alpha + \left(\frac{g_X Q_X(\Phi_s)}{g_Z Q_Y(\Phi)} \right)^2 \frac{v_s}{v} \cos \alpha \cos^2 \theta_{\text{NB}} \right\}, \quad (51)$$

and

$$b = \sin \theta_{\text{NB}} - \epsilon \tan \theta_{\text{W}} \cos \theta_{\text{NB}}. \quad (52)$$

Further,

$$\sigma_{\psi\bar{\psi} \rightarrow SS^\dagger} = \frac{(g_X^2 Q_X(\psi) Q_X(S) \cos^2 \theta_{\text{NB}})^2 (s - 4M_S^2)}{48\pi (s - M_{Z'}^2)^2} \sqrt{\frac{s - 4M_S^2}{s - 4M_\psi^2}} \left(1 + \frac{2M_\psi^2}{s} \right), \quad (53)$$

where Γ_h, Γ_H (Eqs. (48, 50)) are the decay widths corresponding to the physical scalar fields h, H . In the above, $Q_X(\psi) = 1, Q_X(S) = 2$ and $Q_X(\Phi_s) = \frac{1}{2}$ are the $U(1)_X$ gauge charges of ψ, S and Φ_s respectively while $Q_Y(\Phi) = \frac{1}{2}$ denotes the $U(1)_Y$ charge of Φ (see Table 1). The quantity $g_{hZ'Z'}$ ($g_{HZ'Z'}$) in Eq. (51) represents the coupling between scalar field h (H) and two Z' 's¹². Moreover, the expressions of the coupling terms g_{SSH} and g_{SSh} appearing in Eqs. (48, 50) are given in Eq. (27). In Eqs. (45, 46) the symbol $\langle \dots \rangle$ implies the quantity within the curly bracket is thermally averaged. A general expression of thermally averaged annihilation cross section for the annihilation channel $AA^\dagger \rightarrow B\bar{B}$ is given by [68],

$$\langle \sigma_{AA^\dagger \rightarrow B\bar{B}}^{\text{v}} \rangle = \frac{1}{8M_A^4 T K_2^2 \left(\frac{M_A}{T} \right)} \int_{4M_A^2}^{\infty} \frac{1}{2} \sigma_{AA^\dagger \rightarrow B\bar{B}} (s - 4M_A^2) \sqrt{s} K_1 \left(\frac{\sqrt{s}}{T} \right) ds, \quad (54)$$

where K_1, K_2 are the modified Bessel functions of order 1, 2 and T is the temperature of the Universe. The Extra $\frac{1}{2}$ factor before $\sigma_{AA^\dagger \rightarrow B\bar{B}}$ arises due to the fact that the initial state particles

¹²The expressions of the coupling terms g_{hZZ}, g_{HZZ} can be readily obtained from Eq. (51) by replacing the terms b and $\cos \theta_{\text{NB}}$ with the quantities a (Eq. (37)) and $\sin \theta_{\text{NB}}$ respectively.

of the annihilation channel ($AA^\dagger \rightarrow B\bar{B}$) are not identical (see Refs. [68,69] for more discussions). More specifically, no extra $\frac{1}{2}$ factor would be needed if the particle and its antiparticle involved in the initial state of an annihilation process are identical in nature (*e.g.* Majorana fermion or real scalar field). As mentioned earlier, the quantity $\langle \sigma_{\mathbf{v}_{\psi\bar{\psi} \rightarrow X\bar{X}}} \rangle$ appearing in Eq. (45) is the thermally averaged total annihilation cross section of ψ due to all possible final state particles including both the SM as well as non SM particles. However, ψ can interact with the visible world (SM particles) only through the exchange of Z and Z' bosons. Therefore, resulting annihilation cross section of the channel $\psi\bar{\psi} \rightarrow Y\bar{Y}$ (Y is any SM particle except the Higgs boson h and Z boson¹³) is proportional to $\sin^2 \theta_{\text{NB}}$, sine of the mixing angle between the two neutral gauge bosons. Now for small values of θ_{NB} , which is required to satisfy experimental constraints [57], one can use the approximation $\sin \theta_{\text{NB}} \simeq \theta_{\text{NB}}$. Thus, under this circumstance the term $\sin \theta_{\text{NB}} \propto \epsilon$, the kinetic mixing parameter between $U(1)_Y$ and $U(1)_X$ gauge fields (see Eq. (9) for the expression of θ_{NB}). Hence, $\langle \sigma_{\mathbf{v}_{\psi\bar{\psi} \rightarrow X\bar{X}}} \rangle \sim \langle \sigma_{\mathbf{v}_{\psi\bar{\psi} \rightarrow Z'Z'}} \rangle$ as the value of $\chi = \frac{\epsilon}{\cos \theta_{\text{W}}}$ ¹⁴ is severely constrained to be very small [43, 48, 49, 57], which implies that the probability of producing two Z' in the final state is much more than that for the SM particles from the self annihilation of the dark matter candidate ψ . Hence, we can neglect the contributions arising from the annihilation channels $\psi\bar{\psi} \rightarrow Y\bar{Y}$ in Eq. (45).

Let us introduce two dimensionless variables namely $Y_i = \frac{n_i}{s}$ and $x_i = \frac{M_i}{T}$ for $i = \psi, S$. Y_i and M_i are the comoving number density and mass of the dark matter component i . The entropy density of the Universe is denoted by s . In terms of these two dimensionless variables Eq. (45) and Eq. (46) take the following forms,

$$\frac{dY_\psi}{dx_\psi} = - \left(\frac{45G}{\pi} \right)^{-\frac{1}{2}} \frac{M_\psi}{x_\psi^2} \sqrt{g_\star} \left(\langle \sigma_{\mathbf{v}_{\psi\bar{\psi} \rightarrow Z'Z'}} \rangle (Y_\psi^2 - (Y_\psi^{\text{eq}})^2) + \langle \sigma_{\mathbf{v}_{\psi\bar{\psi} \rightarrow SS^\dagger}} \rangle \left(Y_\psi^2 - \frac{(Y_\psi^{\text{eq}})^2}{(Y_S^{\text{eq}})^2} Y_S^2 \right) \right), \quad (55)$$

$$\frac{dY_S}{dx_S} = - \left(\frac{45G}{\pi} \right)^{-\frac{1}{2}} \frac{M_S}{x_S^2} \sqrt{g_\star} \left(\langle \sigma_{\mathbf{v}_{SS^\dagger \rightarrow X\bar{X}}} \rangle (Y_S^2 - (Y_S^{\text{eq}})^2) - \langle \sigma_{\mathbf{v}_{\psi\bar{\psi} \rightarrow SS^\dagger}} \rangle \left(Y_\psi^2 - \frac{(Y_\psi^{\text{eq}})^2}{(Y_S^{\text{eq}})^2} Y_S^2 \right) \right), \quad (56)$$

where G is the Gravitational constant. The quantity g_\star is defined as [68],

$$\sqrt{g_\star} = \frac{h_{\text{eff}}(T)}{\sqrt{g_{\text{eff}}(T)}} \left(1 + \frac{1}{3} \frac{d \ln(h_{\text{eff}}(T))}{d \ln(T)} \right), \quad (57)$$

¹³For ZZ final state $\sigma_{\mathbf{v}_{\psi\bar{\psi} \rightarrow ZZ}}$ is proportional to $\sin^4 \theta_{\text{NB}}$.

¹⁴In this work we adopt $\epsilon \sim 10^{-3}$ which satisfy all the constraints mentioned in the previous section.

with $g_{\text{eff}}(T)$ and $h_{\text{eff}}(T)$ are the effective degrees of freedom corresponding to the energy and entropy densities of the Universe. They are related to energy and entropy densities through the relations $\rho = g_{\text{eff}}(T) \frac{\pi^2}{30} T^4$, $s = h_{\text{eff}}(T) \frac{2\pi^2}{45} T^3$.

We have solved Eqs. (55, 56) numerically to obtain the values of comoving number densities (Y_ψ, Y_S) for both the dark matter components ψ and S respectively at the present temperature T_0 of the Universe. Using these values of Y_i ($i = \psi, S$) at T_0 the relic density of each dark matter component can then be computed using the following equation [70, 71]

$$\Omega_i h^2 = 2.755 \times 10^8 \left(\frac{M_i}{\text{GeV}} \right) Y_i(T_0) . \quad (58)$$

The total relic density ($\Omega_{\text{T}} h^2$) of the dark matter is simply the sum of the relic densities of each dark matter component which can be written as [40],

$$\Omega_{\text{T}} h^2 = \Omega_\psi h^2 + \Omega_S h^2 . \quad (59)$$

4 Results

In this section we describe the effects of the model parameters namely $M_S, M_\psi, M_H, M_{Z'}, \alpha, \lambda_2, \lambda_3$ on the relic densities of both the dark matter components. In this present two component dark matter scenario the role of heavier dark matter candidate is played by the component ψ . Hence, throughout the work we assume $M_\psi > M_S$ and the value of M_S is taken in the range $30 \sim 40$ GeV as this would be required to explain the observed γ -ray excess, from the regions close to the GC, at an energy range $1 \sim 3$ GeV by the annihilation of the dark matter component S . The ranges of the model parameters adopted in this work are given below,

$$\begin{aligned} 1.0 \times 10^{-3} &\leq \lambda_2, \lambda_3 \leq 1.0 \times 10^{-2} , \\ 1.0 \times 10^{-2} &\leq \alpha < 1.4 \times 10^{-1} , \\ 30 \text{ GeV} &\leq M_{Z'} \leq 75 \text{ GeV} , \\ 40 \text{ GeV} &\leq M_H \leq 100 \text{ GeV} , \\ 60 \text{ GeV} &\leq M_\psi \leq 150 \text{ GeV} , \\ 30 \text{ GeV} &\leq M_S \leq 40 \text{ GeV} . \end{aligned} \quad (60)$$

From now on, whenever we use any specific values of the model parameters, we mention it explicitly with the other parameters scanned over their entire considered range given in Eq. (60). Moreover in this work, we have considered $\epsilon \sim 10^{-3}$ which is equivalent to the kinetic mixing parameter $\chi \sim 1.13 \times 10^{-3}$. The corresponding $Z - Z'$ mixing angle lies in the range $\sim (0.6 - 1.65) \times 10^{-3}$ rad for the variation of the entire considered range of $M_{Z'}$ mentioned above.

We have checked that both the values of kinetic mixing parameter and mixing angle θ_{NB} satisfy all the relevant constraints listed in Section 2. In order to study the variations of the relic densities of each of the dark matter components, namely S and ψ , with the model parameters mentioned above, we define a ratio $\frac{\Omega_i h^2}{\Omega_{\text{T}} h^2}$ which represents the fractional contribution of the dark matter component i ($i = S, \psi$) to the overall dark matter relic density ($\Omega_{\text{T}} h^2$). As mentioned earlier, for the computations of individual relic densities ($\Omega_i h^2$) of both the dark matter candidates we need to solve two coupled Boltzmann equations (Eqs. (55), (56)) numerically using Eqs. (47-54) and Eq. (57).

In left panel of Fig. 3 we plot the variations of the fractional contributions of both the dark matter components ψ and S with gauge coupling g_{X} of $U(1)_{\text{X}}$ gauge group for $M_S = 35$ GeV, $M_\psi = 100$ GeV, $M_{Z'} = 50$ GeV and $M_H = 75$ GeV. From the left panel of Fig. 3 it is seen that the fractional contribution $\frac{\Omega_\psi h^2}{\Omega_{\text{T}} h^2}$ ($\frac{\Omega_S h^2}{\Omega_{\text{T}} h^2}$) of the dark matter component ψ (S) decreases (increases) with gauge coupling g_{X} . This nature can be explained from the fact that the annihilation cross section of ψ into $Z'Z'$ final state is directly proportional to g_{X}^4 (see Eq. (47)). Therefore, as the gauge coupling g_{X} increases the annihilation cross section of ψ for the channel $\psi\bar{\psi} \rightarrow Z'Z'$ increases which in turn decreases the relic density of the dark matter component ψ . On the other hand, the coupling term between the two coupled Boltzmann equations (Eq. (56, 55)) is proportional to the annihilation cross section $\sigma_{\nu_\psi\bar{\psi} \rightarrow SS^+}$ which is also directly proportional to g_{X}^4 (see Eq. (53)). Now, any increment in g_{X} will naturally increase the quantity $\sigma_{\nu_\psi\bar{\psi} \rightarrow SS^+}$ and hence the coupling strength between the two coupled Boltzmann equations gets amplified which further reduces the contribution of the heavier component ψ to the total DM relic density. Physically it indicates more and more S particles production in the final state from the pair annihilation of the heavier dark matter component ψ . Consequently, the individual relic density of the lighter DM component S as well as its the fractional contribution to the total DM relic density increases. The variations of the fractional relic density contribution of S with the neutral scalars mixing angle α are shown in the right panel of Fig. 3. In this plot (right panel of Fig. 3) the red coloured region describes the allowed zone in the $\frac{\Omega_S h^2}{\Omega_{\text{T}} h^2}$ -Vs- α plane which satisfies all the constraints listed in Section 2 for $M_S = 30$ GeV, $M_H = 65$ GeV while the green coloured region is for the case when $M_S = 35$ GeV, $M_H = 75$ GeV. Both of these plots are computed for heavier dark matter mass $M_\psi = 100$ GeV and $M_{Z'} = 50$ GeV. From the right panel of Fig. 3 it is evident that in order to satisfy all the relevant constraints listed in Section 2, the maximum allowed value of the neutral scalars mixing angle α is ~ 0.07 rad.

We also calculate the variations of the ratios $\frac{\Omega_S h^2}{\Omega_{\text{T}} h^2}$, $\frac{\Omega_\psi h^2}{\Omega_{\text{T}} h^2}$ with the mass of the lighter dark matter component S for two different values of M_ψ and the results are plotted in both the panels

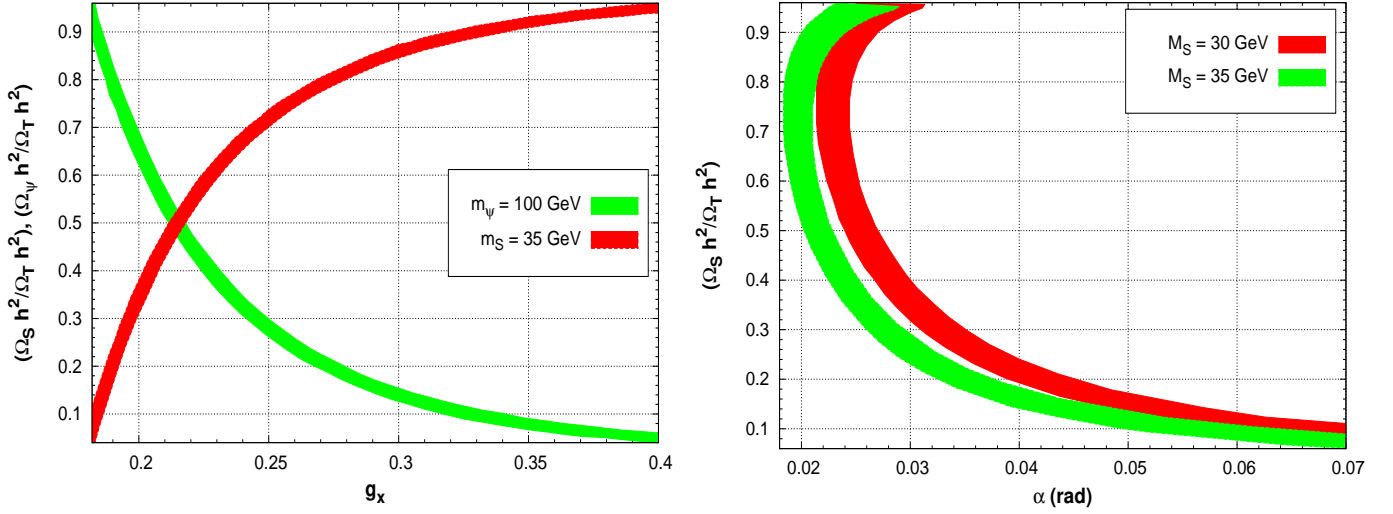


Figure 3: Left panel : Variations of $\frac{\Omega_S h^2}{\Omega_T h^2}$, $\frac{\Omega_\psi h^2}{\Omega_T h^2}$ with the gauge coupling g_X for $M_S = 35$ GeV and $M_\psi = 100$ GeV. Right Panel : Variations of $\frac{\Omega_S h^2}{\Omega_T h^2}$ with the mixing angle α between the neutral scalars h, H for $M_S = 30$ GeV, $M_\psi = 100$ GeV and $M_S = 35$ GeV, $M_\psi = 100$ GeV respectively.

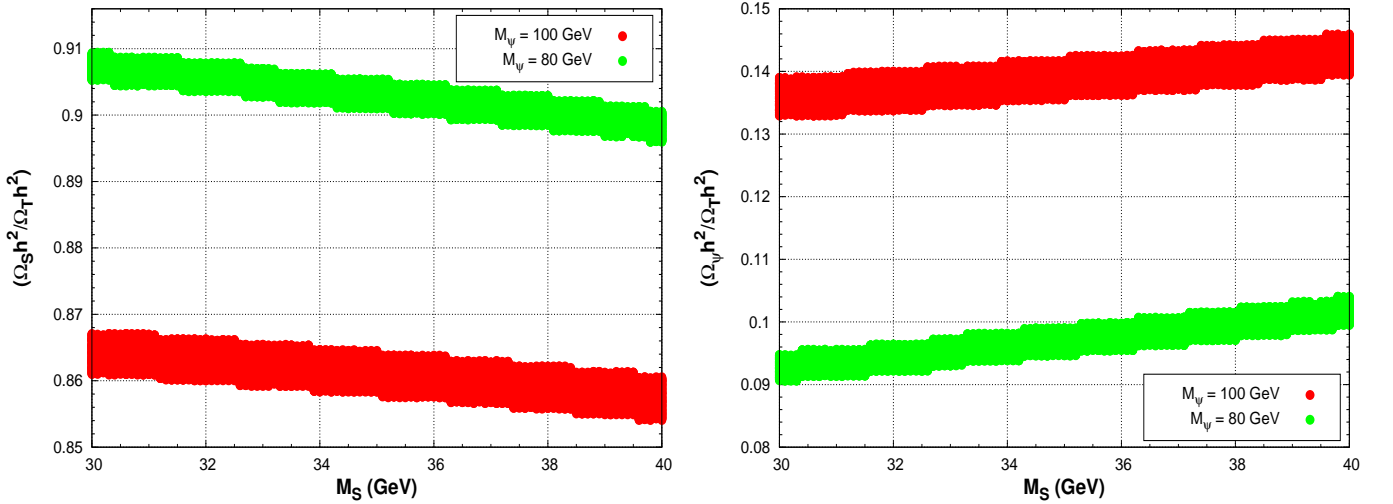


Figure 4: Variations of $\frac{\Omega_S h^2}{\Omega_T h^2}$ (left panel) and $\frac{\Omega_\psi h^2}{\Omega_T h^2}$ (right panel) with the mass of S for $M_\psi = 80$, 100 GeV respectively.

of Fig.4. In the left panel of Fig. 4 we show the variations of the fractional contribution of S to the total dark matter relic density with M_S for $M_\psi = 80$ GeV (green coloured band) and 100 GeV (red coloured band). The right panel of the same figure (Fig. 4) shows how the fractional contribution of the heavier dark matter component ψ to the total relic density varies with the

mass of lighter dark matter component S . Similar to the plots in the left panel of Fig. 4, in the right panel too, the green and red coloured band represent allowed zones for $M_\psi = 80$ GeV and 100 GeV respectively. From the left panel of Fig. 4 it appears that the contribution of S to the overall DM relic density decreases as its mass increases. A possible reason could be the increase of annihilation cross section ($\sigma v_{SS^\dagger \rightarrow f\bar{f}}$) of the dark matter component S into the final states comprised of fermion and antifermion pair ($SS^\dagger \rightarrow f\bar{f}$, f being any SM fermion except top quark) with M_S (see Eq. (48)). Therefore the relic density of S decreases. This reduction in $\Omega_S h^2$ must be compensated by an increment towards the relic density of ψ such that the total relic density of both the dark matter candidates always lies within the range provided by the PLANCK experiment. Also, the annihilation cross section of ψ for the channel $\psi\bar{\psi} \rightarrow SS^\dagger$ decreases with M_S (see Eq. (53)) which further increases the individual density of ψ and hence, its the contribution to the overall density. This feature is revealed in the plots of the right panel of Fig. 4.

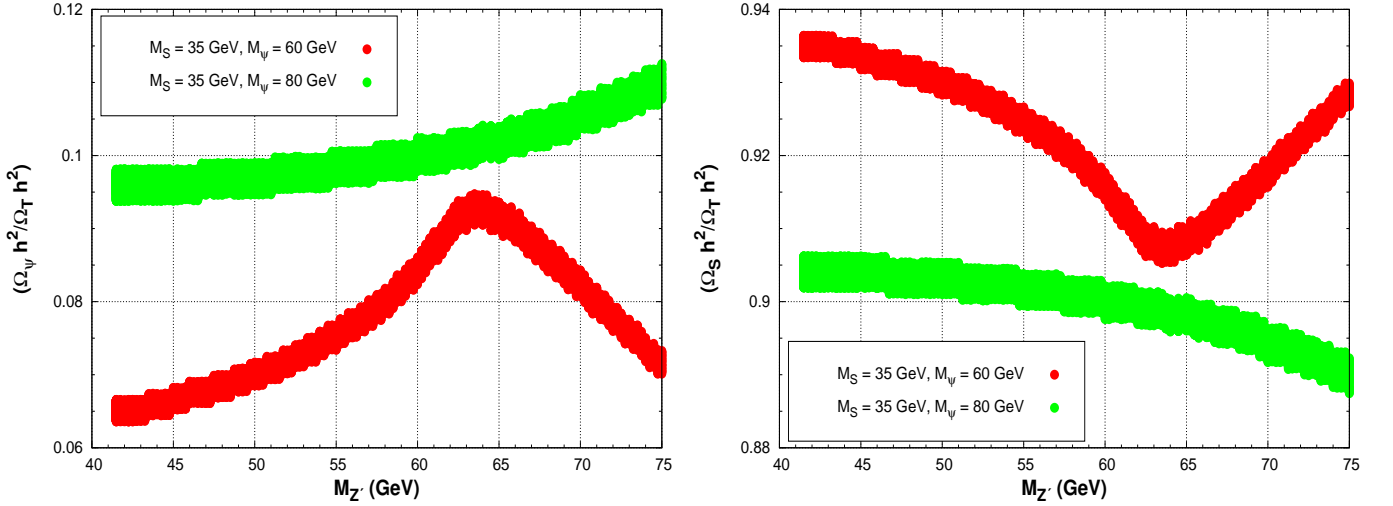


Figure 5: Variations of $\frac{\Omega_\psi h^2}{\Omega_T h^2}$ (left panel) and $\frac{\Omega_S h^2}{\Omega_T h^2}$ (right panel) with the mass ($M_{Z'}$) of Z' for two different values of $M_\psi = 60$ GeV, 80 GeV while M_S remains fixed at 35 GeV.

It has been discussed earlier that the dark matter component ψ can interact with both the visible (SM particles) and invisible (other dark matter component S) world mainly through the exchange of gauge boson Z' . Therefore, the number density of the heavier dark matter component ψ at present epoch (the relic density of ψ) should depend on the mass of Z' . The two main annihilation channels (see Fig. 2) of ψ behave exactly the opposite way with respect to the variation of $M_{Z'}$ and $\psi\bar{\psi} \rightarrow Z'Z'$ being its dominant annihilation mode. While the annihilation

cross section for the channel $\psi\bar{\psi} \rightarrow Z'Z'$ (Eq. (47)) decreases with $M_{Z'}$, the same quantity (Eq. (53)) for the interaction mode in which heavier dark matter components annihilate to produce lighter dark matter components ($\psi\bar{\psi} \rightarrow SS^\dagger$) increases with the mass of Z' boson as long as $M_{Z'} < \sqrt{s}$ ¹⁵ condition holds. Hence, the present day abundance of the dark matter component ψ is guided by the combined effects of both the above mentioned annihilation processes. In left panel of Fig. 5 we show the variation of fractional relic density of ψ with the mass of Z' . The red coloured band is for $M_\psi = 60$ GeV while the variation of $\frac{\Omega_\psi h^2}{\Omega_{\text{T}} h^2}$ for $M_\psi = 80$ GeV is represented by green coloured band. From this figure it is seen that for $M_\psi = 60$ GeV, the quantity $\frac{\Omega_\psi h^2}{\Omega_{\text{T}} h^2}$ initially increases with $M_{Z'}$ (when $M_{Z'} \lesssim 63$ GeV) and thereafter it decreases as $M_{Z'}$ goes beyond 63 GeV. A possible reason of this nature could be when $s \geq 4M_{Z'}^2$, $\psi\bar{\psi} \rightarrow Z'Z'$ is the dominant annihilation mode of ψ , therefore the fractional relic density of ψ enhances with the increase of $M_{Z'}$. However for $s < 4M_{Z'}^2$, the DM component ψ annihilates only through the channel $\psi\bar{\psi} \rightarrow SS^\dagger$ as the annihilation process $\psi\bar{\psi} \rightarrow Z'Z'$ is now kinematically forbidden. Consequently, with respect to the variation of $M_{Z'}$ the ratio $\frac{\Omega_\psi h^2}{\Omega_{\text{T}} h^2}$ changes in the opposite direction as compared to the former case. On the other hand for $M_\psi = 80$ GeV and above, s is always greater than $4M_{Z'}^2$, therefore the interaction mode $\psi\bar{\psi} \rightarrow Z'Z'$ is always kinematically accessible. Hence for the entire considered range of $M_{Z'}$, the fractional contribution of ψ towards the total DM relic density increases with the mass of Z' . The change in the mass of the Z' boson has no significant effect on the interactions of the lighter dark matter component S with the SM fermions as those occur mainly through the exchange of neutral scalars namely h and H . However, the changes occur in $\Omega_\psi h^2$ due to the variation of $M_{Z'}$ should be compensated by an equal and opposite changes in the relic density of the DM component S such that the total relic density should always satisfies the range predicted by the satellite borne experiment PLANCK. This is shown in the right panel of Fig. 5 where the variation of fractional relic density of S with $M_{Z'}$ are plotted. Both the plots in Fig. 5 have been computed for a fixed value of $M_S = 35$ GeV.

Left panel of Fig. 6 describes the variations of the ratio $\frac{\Omega_\psi h^2}{\Omega_{\text{T}} h^2}$ with the heavier dark matter mass (M_ψ) for different values of the gauge coupling g_X and the mass (M_S) of S . The red band represents the variations for $g_X = 0.25$, $M_S = 35$ GeV while the green and blue coloured bands are for two different values of M_S namely, 30 and 35 GeV respectively with the same gauge coupling $g_X = 0.30$. From this figure (left panel of Fig. 6) it appears that the contribution of the heavier dark matter component ψ to the overall dark matter density increases with its mass M_ψ . However, the ratio $\frac{\Omega_\psi h^2}{\Omega_{\text{T}} h^2}$ decreases with g_X and remains nearly same for the variations of the mass of the lighter dark matter component S from 30 GeV to 35 GeV. This increment of

¹⁵which is the case we are considering.

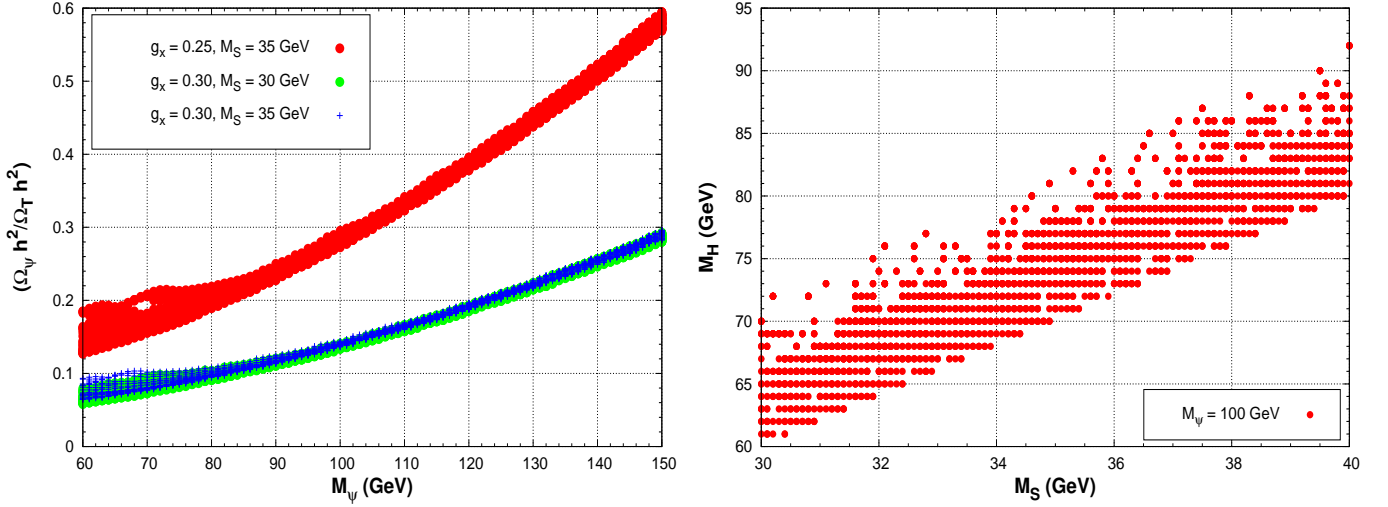


Figure 6: Left panel : Variations of the fractional contributions of the dark matter component ψ with its mass M_ψ for different values of the gauge coupling g_X and the mass of S (M_S). Right panel : Variations of the allowed ranges of M_H with M_S while the mass of heavier dark matter is fixed at 100 GeV.

$\frac{\Omega_\psi h^2}{\Omega_T h^2}$ is evident from Eqs. (47, 53) which indicate that the annihilation cross sections of ψ for the channels $\psi\bar{\psi} \rightarrow Z'Z', SS^\dagger$ decrease with M_ψ . On the other hand as the annihilation cross sections of these two channels are proportional to g_X^4 therefore the fractional contribution of ψ to the total relic density decreases with g_X . The right panel of Fig. 6 represents how the range of allowed values of M_H vary with the mass of S for $M_\psi = 100$ GeV. Needless to mention that, for not only each point in the right panel of Fig. 6 but for every other plots given in both panels of Figs. 3 - 6, all the possible constraints discussed in the Section 2 namely, the vacuum stability bounds, the relic density constraints, the constraints obtain from the results of dark matter direct detection experiments and LHC etc. are always satisfied.

Signal strength of the scalar H - We have also computed the signal strength of the scalar boson H for its various allowed decay channels ($H \rightarrow X\bar{X}$). The signal strength ($R'_{X\bar{X}}$) of H for a particular decay mode is defined as the ratio of production cross section times the branching ratio of that decay channel of H with the SM expectation of these quantities. Thus the signal strength of H can be expressed as

$$R'_{X\bar{X}} = \frac{\sigma_H}{\sigma_H^{\text{SM}}} \frac{\text{BR}(H \rightarrow X\bar{X})}{\text{BR}(H \rightarrow X\bar{X})^{\text{SM}}}, \quad (61)$$

In the left panel of Fig. 7 we show the variation of signal strength ($R'_{X\bar{X}}$) of the scalar boson H for a particular decay channel $H \rightarrow X\bar{X}$ (X is any SM particle) with the allowed range of the mixing angle α between h and H obtained from right panel of Fig. 3. The variation of

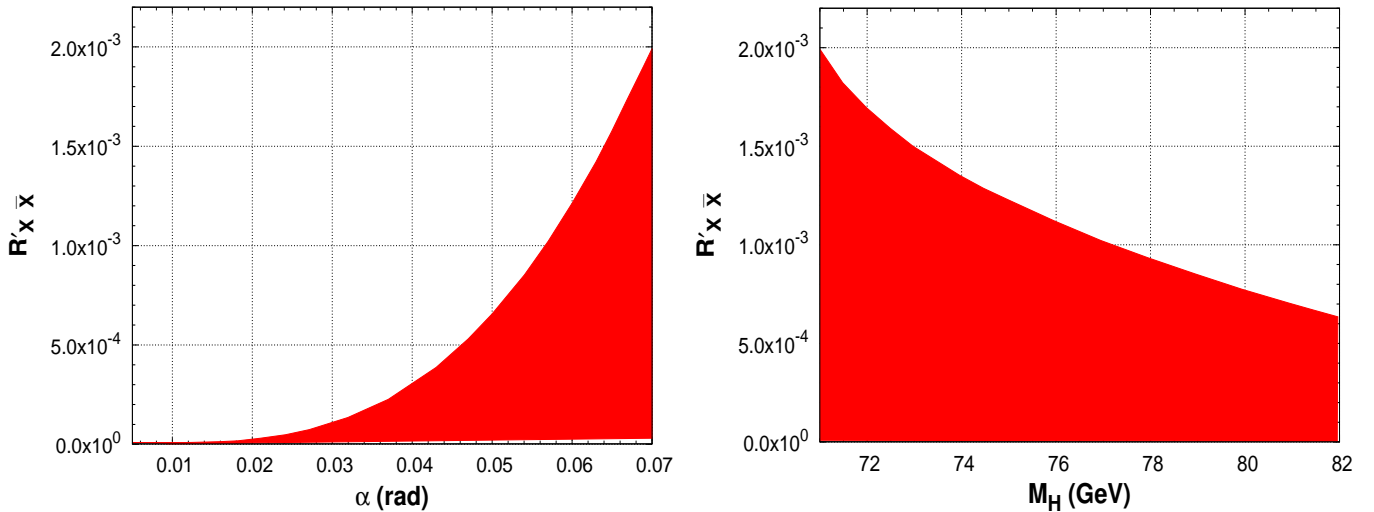


Figure 7: Left (Right) panel- Variation of signal strength of the scalar boson H for a particular decay channel $H \rightarrow X\bar{X}$ with mixing angle α (mass M_H of H). Here X is any SM particle.

the same quantity ($R'_{X\bar{X}}$) with the mass¹⁶ of H is also shown in the right panel of Fig. 7. The increase of $R'_{X\bar{X}}$ with α is due to the fact that coupling strength of H with any SM particle X is proportional to the mixing angle α . It is evident from both the plots of Fig. 7 that within the allowed ranges of α and M_H , the signal strength of H is extremely weak and its value is $\lesssim 2 \times 10^{-3}$ in units of the Standard Model production cross section of H .

We have already discussed in the Section 2 that in order to compare the direct detection results computed using a multicomponent dark matter model, one should rescale the spin independent scattering cross sections for both the dark matter components by an appropriate factor (see Eq. (28)) which manifests the existence of multicomponent dark matter. In view of this, the spin independent “effective scattering cross sections” between each of the dark matter candidate (S , ψ) and the nucleon are plotted in Fig. 8. Here red coloured zone represents $\sigma_{\text{SI}}^{iN \rightarrow iN}$ for the candidate S ($i = S$) however, for the heavier dark matter candidate ψ ($i = \psi$) it is indicated by the green coloured band. For the comparison with the latest direct detection experimental results the data [46] obtained from the LUX experiment are superimposed on the same figure (Fig. 8). From the Fig. 8 it is seen that although some portions, only for the lighter DM component S , in the $\sigma_{\text{SI}} - M_{\text{DM}}$ plane are already excluded by the LUX experiment, still there exist enough

¹⁶These plots are drawn for the mass of the lighter dark matter particle $M_S = 35$ GeV. We have shown earlier (right panel of Fig. 6) that for $M_S = 35$ GeV, both the relic density as well as the direct detection criteria are simultaneously satisfied only when M_H lies between ~ 70 GeV to 82 GeV.

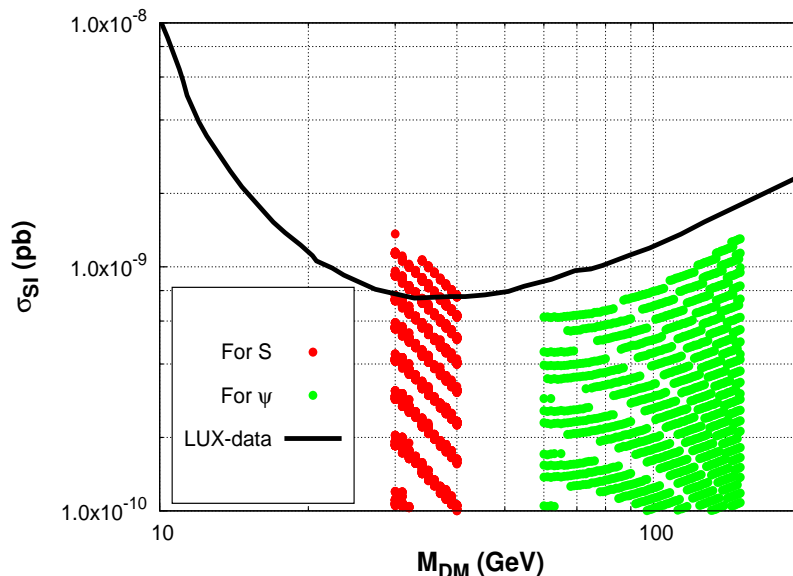


Figure 8: Spin independent “effective scattering cross sections” of the dark matter component S (red coloured region) and ψ (green coloured region). Limits obtained from LUX experiment are denoted by black solid line.

allowed regions in the $\sigma_{\text{SI}} - M_{\text{DM}}$ plane for both the dark matter components S and ψ which can be tested by more sensitive (“ton-scale”) direct detection experiments in near future.

In Table 2 we show the ranges of values of different observable quantities, namely α , θ_{NB} , $R_{X\bar{X}}$, $R'_{X\bar{X}}$, BR_{inv} , Γ_h , Γ_H , $\frac{\Omega_S h^2}{\Omega_{\text{T}} h^2}$, $\frac{\Omega_\psi h^2}{\Omega_{\text{T}} h^2}$, $\sigma'_{\text{SI}}{}^{SN \rightarrow SN}$, $\sigma'_{\text{SI}}{}^{\psi N \rightarrow \psi N}$, which are allowed by various theoretical, observational and experimental constraints listed in Section 2. These ranges are obtained for the chosen values of the kinetic mixing parameter $\epsilon = 1.0 \times 10^{-3}$ and the $U(1)_X$ gauge coupling $g_X = 0.3$. The other relevant model parameters namely M_S , M_ψ , $M_{Z'}$, M_H , $\lambda_{2,3}$, required for computing these allowed ranges of different observables, are varied over their entire ranges mentioned in Eq. (60).

5 1-3 GeV γ excess from Galactic Centre.

In this section our endeavour is to explain recently observed excess γ -rays at an energy range 1-3 GeV by Fermi-LAT from the Galactic Centre region within the framework of the proposed two component dark matter model. In the present two component DM scenario, lighter dark matter component namely, S having mass in the range $30 \sim 40$ GeV annihilates with its own antiparticle S^\dagger and thereby produces $b\bar{b}$ pair in the final state with branching ratio $\sim 85\% - 90\%$.

α (rad)	θ_{NB} (rad)	$R_{X\bar{X}}$	$R'_{X\bar{X}}$	BR_{inv} of h	Γ_h (GeV)
$\lesssim 7.0 \times 10^{-2}$	$\sim (0.6 - 1.65) \times 10^{-3}$	$\gtrsim 0.80$	$\lesssim 2.0 \times 10^{-3}$	$\lesssim 20\%$	$\sim (4.1 - 5.1) \times 10^{-3}$
Γ_H (GeV)	$\frac{\Omega_S h^2}{\Omega_{\text{T}} h^2}$	$\frac{\Omega_\psi h^2}{\Omega_{\text{T}} h^2}$	$\sigma'_{\text{SI}}{}^{SN \rightarrow SN}$ (pb)	$\sigma'_{\text{SI}}{}^{\psi N \rightarrow \psi N}$ (pb)	
$\sim (0.08 - 2.3) \times 10^{-4}$	$\sim 0.7 - 0.94$	$\sim 0.06 - 0.3$	$\sim (0.1 - 0.8) \times 10^{-9}$	$\sim (0.1 - 1.3) \times 10^{-9}$	

Table 2: Allowed ranges of various observable quantities computed using the present two component DM model for $\epsilon = 1.0 \times 10^{-3}$, $g_X = 0.3$. Other relevant model parameters, required for this computation, are scanned over their entire considered ranges mentioned in Eq. (60).

Thereafter those b-quarks hadronise to produce γ -rays that can be detected by Fermi-LAT. The annihilation process ($SS^\dagger \rightarrow b\bar{b}$) of the dark matter component S proceeds mainly through the exchange of SM like Higgs boson h and H . The Feynman diagram for this annihilation process is shown in the left panel of Fig. 2. The differential γ -ray flux due to self annihilation of S in the GC region is given by [72]¹⁷,

$$\frac{d\Phi_\gamma}{d\Omega dE} = \frac{r_\odot}{8\pi} \left(\frac{\rho_\odot}{M_S} \right)^2 \bar{J} \langle \sigma_{\text{V}}{}^{SS^\dagger \rightarrow b\bar{b}} \rangle' \frac{dN_\gamma^b}{dE}, \quad (62)$$

where $\frac{dN_\gamma^b}{dE}$ is the energy spectrum of photons produced from the hadronisation processes of b quarks¹⁸. We have used the numerical values of the photon spectrum for different values of photon energy E_γ , given in Ref. [72]. In the above $\rho_\odot = 0.3 \text{ GeV/cm}^3$ is the dark matter density at the solar location which is nearly $r_\odot \simeq 8.5 \text{ kpc}$ away from the Galactic Centre. The quantity \bar{J} for the case of dark matter annihilation in the GC can be expressed as,

$$\bar{J} = \frac{4}{\Delta\Omega} \int \int db dl \cos b J(b, l), \quad (63)$$

¹⁷In Ref. [72], there is an extra half factor in the expression of differential γ -ray flux (Eq. (62)) originating from the annihilation of dark matter particle which is not its own antiparticle. In our case, as already mentioned before, the lighter dark matter candidate is represented by a complex scalar field S . Hence, S is not self conjugate and the extra half factor which should be present in Eq. (62) due to the nature of dark matter particle is already taken into account when we have define the expression of thermally averaged annihilation cross section of S (see Eq. (54) for the definition of $\langle \sigma_{\text{V}}{}^{SS^\dagger \rightarrow b\bar{b}} \rangle$).

¹⁸originate from the self annihilation of S through the process $SS^\dagger \rightarrow b\bar{b}$.

with

$$J(l, b) = \int_{\text{l.o.s}} \frac{d\mathfrak{s}}{r_\odot} \left(\frac{\rho(r)}{\rho_\odot} \right)^2, \quad (64)$$

and

$$\Delta\Omega = 4 \int dl \int db \cos b, \quad (65)$$

$$r = (r_\odot^2 + \mathfrak{s}^2 - 2r_\odot \mathfrak{s} \cos b \cos l)^{1/2}. \quad (66)$$

In Eqs. (63, 65, 66), l and b represent the galactic longitude and latitude respectively. While computing the values of \bar{J} we perform the integral over a region which is situated within a radius of 5° [10] around the GC. Integral over \mathfrak{s} in Eq. (64) is along the line of sight (l.o.s) distance. The quantity $\langle\sigma v_{SS^\dagger \rightarrow b\bar{b}}\rangle'$ in Eq. (62) is the ‘‘effective annihilation cross section’’ which is in the product of annihilation cross section of the channel $SS^\dagger \rightarrow b\bar{b}$ and square of the contribution of the component S to the total dark matter relic density ($\Omega_{\text{T}}h^2$) *i.e.*

$$\langle\sigma v_{SS^\dagger \rightarrow b\bar{b}}\rangle' = \xi_S^2 \langle\sigma v_{SS^\dagger \rightarrow b\bar{b}}\rangle, \quad (67)$$

where

$$\xi_S = \frac{\Omega_S}{\Omega_{\text{T}}} \quad (68)$$

is the fractional relic density of the component S . The use of $\langle\sigma v_{SS^\dagger \rightarrow b\bar{b}}\rangle'$ (‘‘effective annihilation cross section’’) instead of actual annihilation cross section for the channel $SS^\dagger \rightarrow b\bar{b}$ ($\langle\sigma v_{SS^\dagger \rightarrow b\bar{b}}\rangle$) in Eq. (62) is needed since we are working in a framework with more than one component of the dark matter. Note that if the entire dark sector is composed of only one type of particle (say S) then $\xi_S = 1$, therefore $\langle\sigma v_{SS^\dagger \rightarrow b\bar{b}}\rangle'$ and $\langle\sigma v_{SS^\dagger \rightarrow b\bar{b}}\rangle$ are identical. The expression of $\langle\sigma v_{SS^\dagger \rightarrow b\bar{b}}\rangle$ is given in Eq. (48) of Section 3. Computation of γ -ray flux using Eq. (62) requires the nature of the variation of the dark matter density in the neighbourhood regions of the Galactic Centre with the distance r . In short one needs to know the DM halo profile $\rho(r)$ as a function of r . In the present work we use the NFW profile [73] with $\gamma = 1.26$ [10]. The general expression of NFW profile is given by,

$$\rho_{\text{NFW}} = \rho_s \frac{\left(\frac{r}{r_s}\right)^{-\gamma}}{\left(1 + \frac{r}{r_s}\right)^{3-\gamma}}, \quad (69)$$

where scale radius $r_s = 20$ Kpc. The normalisation constant ρ_s (scale density) is obtained by demanding that at the solar location ($r = r_\odot$) the dark matter density should be 0.3 GeV/cm^3 .

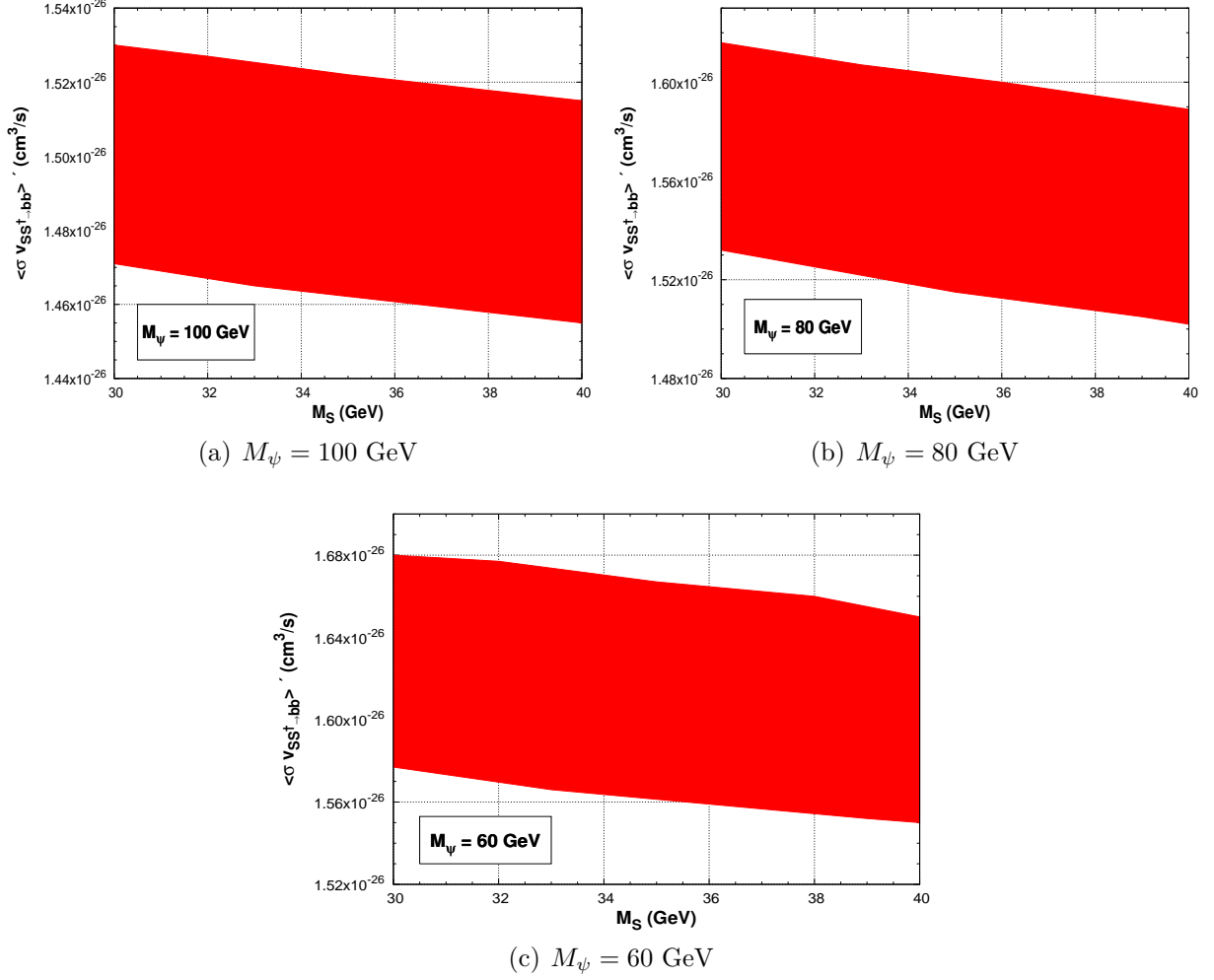
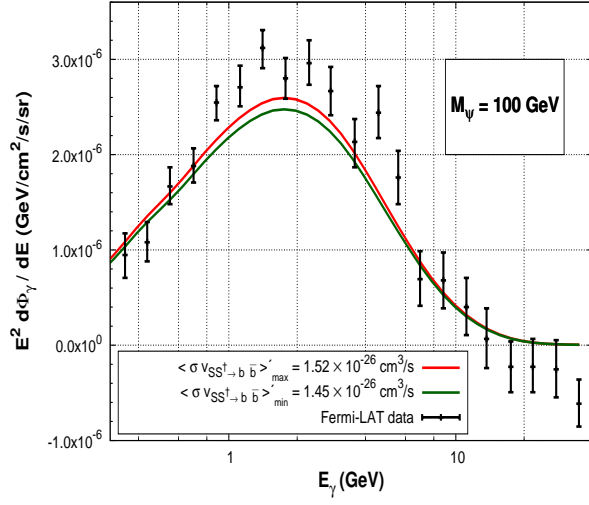
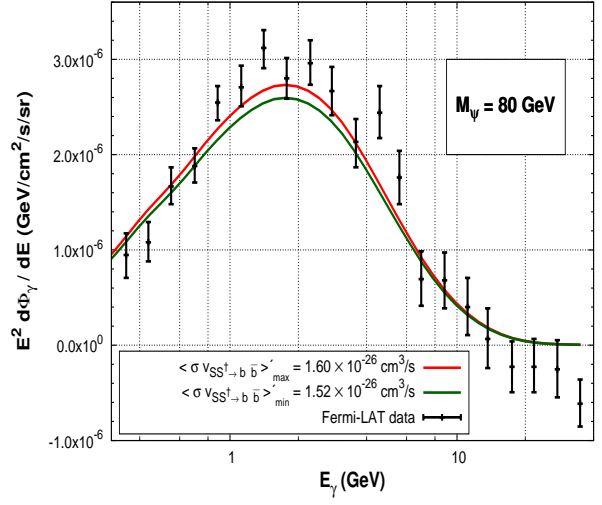


Figure 9: Left-Panel : Variations of $\langle \sigma v_{SS^\dagger \rightarrow b\bar{b}} \rangle'$ with the mass of the dark matter component S for different values of the mass of heavier dark matter component ψ .

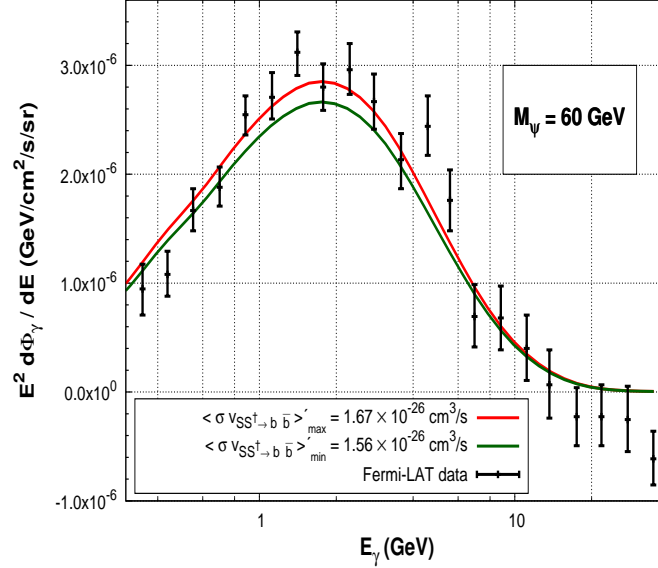
In Fig. 9(a-c) we show the variations of the “effective annihilation cross section” $\langle \sigma v_{SS^\dagger \rightarrow b\bar{b}} \rangle'$ (defined in Eq. (67)) for annihilation channel $SS^\dagger \rightarrow b\bar{b}$ with the mass of the the dark matter component S in the range of 30 GeV - 40 GeV for three different values of M_ψ , namely, 60, 80 and 100 GeV. Since the quantity $\langle \sigma v_{SS^\dagger \rightarrow b\bar{b}} \rangle'$ is the product of annihilation cross section of S for the channel $SS^\dagger \rightarrow b\bar{b}$ and square of the fractional contribution of S to the total relic density (ξ_S^2) (see Eq. (67)), therefore in all the plots (a-c) of Fig. 9 we have taken only those values of both the quantities $\langle \sigma v_{SS^\dagger \rightarrow b\bar{b}} \rangle'$ and ξ_S for which the total dark matter density lies within the range predicted by the PLANCK experiment (Eq. (24)). All the plots in Fig. 9 show that the “effective annihilation cross section” of the channel $SS^\dagger \rightarrow b\bar{b}$ decreases as the mass (M_ψ) of the heavier dark matter component increases. From Eq. (59) and Eq. (68) we know that



(a) $M_{\psi} = 100 \text{ GeV}$



(b) $M_{\psi} = 80 \text{ GeV}$



(c) $M_{\psi} = 60 \text{ GeV}$

Figure 10: Variations of γ -ray flux obtain from the annihilation of S in the Galactic Centre as a function of the photon energy (E_{γ}) for three different values of M_{ψ} .

the fractional contributions of both the dark matter components namely, ψ and S are related through the relation

$$\xi_{\psi} + \xi_S = 1 . \quad (70)$$

Now, ξ_{ψ} increases with M_{ψ} (see left panel of Fig. 6) therefore in order to satisfy the above relation given in Eq. (70) the fraction contribution (ξ_S) of the lighter dark matter component

to the overall density decreases with the increase of heavier dark matter mass. This results in an enhancement in the pair annihilation rate ($\langle\sigma v_{SS^\dagger\rightarrow f\bar{f}}\rangle$, f is any SM fermion except top quark) of the dark matter component S . Since $\langle\sigma v_{SS^\dagger\rightarrow b\bar{b}}\rangle'$ is proportional to ξ_S^2 (see Eq. (67)) hence, the “effective annihilation cross section” of S for the channel $SS^\dagger \rightarrow b\bar{b}$ decreases with M_ψ . Similarly, one can understand the variations of $\langle\sigma v_{SS^\dagger\rightarrow b\bar{b}}\rangle'$ with the mass of S using left panel of Fig. 4. From all the plots (a-c) of Fig. 9 it appears the “effective annihilation cross section” of the dark matter candidate S for the annihilation channel $SS^\dagger \rightarrow b\bar{b}$ lies within the range $(1.45 \sim 1.68) \times 10^{-26} \text{cm}^3/\text{s}$. This allowed range of $\langle\sigma v_{SS^\dagger\rightarrow b\bar{b}}\rangle'$ falls well below the current bounds on the dark matter annihilation cross section into $b\bar{b}$ final state from collider results and other various measurements like antiproton flux, positron flux, diffuse radio emission, CMB etc. (see left panel of Fig. 1 of Ref. [74]).

The plots (a-c) in Fig. 10 show the variations of the γ -ray flux obtained from the regions surrounding the Galactic Centre due to the self annihilation of the dark matter candidate S of mass 35 GeV into $b\bar{b}$ final state for three different values of $M_\psi = 100, 80$ and 60 GeV respectively. In each of the plots (a-c) of Fig. 10 the red and green solid lines represent the γ -ray fluxes computed by using maximum and minimum allowed values of the “effective annihilation cross section” ($\langle\sigma v_{SS^\dagger\rightarrow b\bar{b}}\rangle'$) for a particular value of the mass of heavier dark matter component ψ . These quantities are represented by $\langle\sigma v_{SS^\dagger\rightarrow b\bar{b}}\rangle'_{\text{max}}$ and $\langle\sigma v_{SS^\dagger\rightarrow b\bar{b}}\rangle'_{\text{min}}$ respectively. The range of allowed values of $\langle\sigma v_{SS^\dagger\rightarrow b\bar{b}}\rangle'$ with the mass of S for three different values of M_ψ ($M_\psi = 60, 80$ and 100 GeV) are given in plots (a-c) of Fig. 9. The black vertical lines in each of the plots of Fig. 10 represent the Fermi-LAT data and corresponding error bars. Since the allowed ranges of the “effective annihilation cross section” of the dark matter particle S for the channel $SS^\dagger \rightarrow b\bar{b}$ decrease with the increase of M_ψ (see plots (a-c) of Fig. 9 and the related discussions), therefore the corresponding γ -ray fluxes (Eq. (62)) shown in Fig. 10 also decrease with M_ψ . Therefore, comparing the gamma-ray fluxes computed for three different values of M_ψ with the Fermi-LAT data, we find that the γ -ray fluxes obtained for $M_\psi = 60$ and 80 GeV agree well with the experimental data. Moreover, the γ -ray fluxes computed for $M_\psi \geq 100$ GeV are incompatible with the available Fermi-LAT data.

We have also compared the range of allowed values of the “effective annihilation cross section” ($\langle\sigma v_{SS^\dagger\rightarrow b\bar{b}}\rangle$) of the dark matter candidate S for the channel $SS^\dagger \rightarrow b\bar{b}$ with the limits obtained from the analyses of both Fermi-LAT collaboration [75] and DES collaboration [76]. In Fig. 11 the dashed blue line represents the upper limits on dark matter annihilation cross section for $b\bar{b}$ annihilation channel. This limit is obtained after a combined analysis of six years of Pass 8 Reprocessed data from 15 dwarf spheroidal galaxies (dSphs) by the Fermi-LAT collaboration.

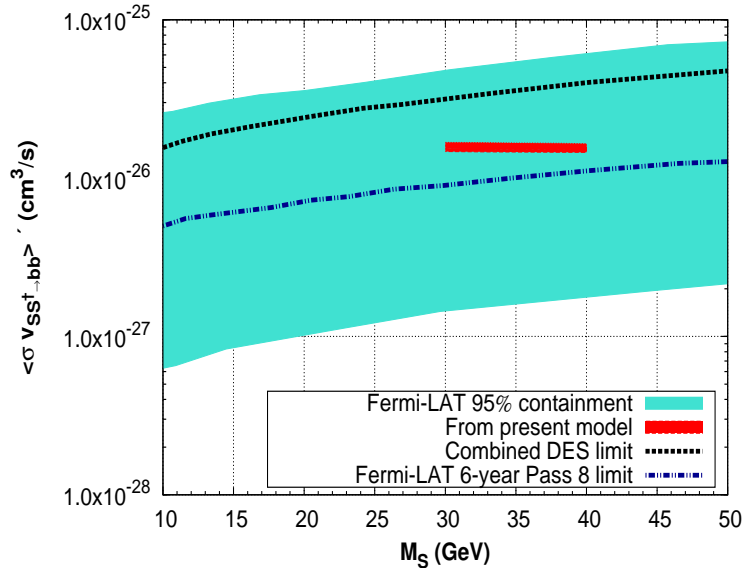


Figure 11: Comparison between the range of allowed values of “effective annihilation cross section” of DM candidate S (for $b\bar{b}$ annihilation channel) obtained from the present model and the 95% C.L. upper limits as well as the corresponding error bar reported by both Fermi-LAT and DES collaborations after their analyses of data from dwarf spheroidal galaxies.

The corresponding 95% C.L. error band is shown by the turquoise coloured contour. The red coloured patch is the range of allowed values of $\langle \sigma v_{S S^\dagger \rightarrow b\bar{b}} \rangle'$ that is derived from the present model for different values of relevant model parameters (see Fig. 9) while the 95% C.L. combined upper limits on $\langle \sigma v_{b\bar{b}} \rangle$, obtained from the analysis of 8 new dSphs by the DES collaboration, is described by the black dashed line. Although it appears from Fig. 11 that the allowed values of $\langle \sigma v_{S S^\dagger \rightarrow b\bar{b}} \rangle'$ obtained from the present two component DM model which produce the observed flux lie above the upper limits given by Fermi-LAT from their analysis of 15 dSphs’s data (blue dashed line), the allowed values of $\langle \sigma v_{S S^\dagger \rightarrow b\bar{b}} \rangle'$ still fall within the 95% C.L. error band reported by Fermi-LAT (turquoise coloured band). Needless to mention here that the range of allowed values of $\langle \sigma v_{S S^\dagger \rightarrow b\bar{b}} \rangle'$ satisfy the limits reported by the DES collaboration (black dashed line). We have also checked the gamma-ray flux from the GC using other dark matter density profile available in literature, namely the Einasto profile [77,78]. We have found that in order to explain the Fermi-LAT observed gamma-ray flux from the self annihilation of a 35 GeV S particle using Einasto dark matter profile, one needs $\langle \sigma v_{S S^\dagger \rightarrow b\bar{b}} \rangle' \sim 4.8 \times 10^{-26} \text{ cm}^3/\text{s}$ which violates both the upper limits reported by Fermi-LAT (blue dashed line in Fig. 11) and DES (black dashed line in Fig. 11) collaborations.

6 Summary

In the present work, we propose a dark matter model which is an extension of the Standard Model of particles physics in all three sectors namely gauge, fermionic as well as scalar and contains two different types of dark matter candidates. Therefore, in this two component dark matter model the role of two dark matter candidates are played by a complex scalar field S and a Dirac fermion ψ respectively. Although, both of these dark sector particles (S, ψ) are singlet under SM gauge group ($SU(3)_c \times SU(2)_L \times U(1)_Y$) but possess a non zero $U(1)_X$ charge which ensures their stability. Thus, in addition to SM gauge group we have an additional local $U(1)_X$ gauge symmetry under which all the SM particles (including the Higgs boson) behave like singlet. Besides the dark matter component S , the scalar sector of the present model is composed of another complex singlet Φ_s and a $SU(2)_L$ doublet (Φ) (the usual Higgs doublet). Both Φ and Φ_s possess non zero VEVs namely, v and v_s respectively which spontaneously break the $SU(2)_L \times U(1)_Y \times U(1)_X$ symmetry to a remnant $U(1)_{em} \times \mathbb{Z}_2$ symmetry. This residual \mathbb{Z}_2 symmetry stabilize the fields S and ψ . As a result of this symmetry breaking, the neutral components of Φ and Φ_s mix with each other and we get two physical scalars, namely h and H with a nonzero mixing between angle α between them. The symmetry breaking phenomenon is manifested by the presence of five gauge bosons in the model such as W^\pm, Z, Z' and A . Among these five gauge bosons only W^\pm has non zero electrical charge and A remains massless which is identified as the “photon” (mediator of the electromagnetic interaction). We have taken into account all the relevant constraints which get affected due to the presence of nonzero mixing angles between both $Z - Z'$ and $h - H$. These include electroweak precision observables, electroweak oblique parameters, ρ parameter, bounds from the LHC results on the signal strength and the invisible decay width of the SM Higgs boson etc. Considering S and ψ as the two possible candidates for the dark matter particles in the Universe, their viability is examined by computing the total relic abundance at the present epoch and the scattering cross sections off the detector nuclei. In order to find the total relic abundance which is the sum of the individual relic abundances of both the dark matter components, we have solved two coupled Boltzmann equations for ψ and S at the present epoch. We find that for a wide range of values of the model parameters the total relic density of the two dark matter candidates falls within the range specified by the PLANCK experiment. We have compared the spin independent “effective scattering cross sections” for both the dark matter candidates off the detector nuclei with the latest results of LUX experiment. We find that although, some portions of only the lighter dark matter component S of present two component dark matter model have already been excluded by the results of LUX experiment but still their exist enough regions in the $\sigma_{SI} - M_{DM}$ plane which can be tested by the “ton-scale” direct detection experiments in near future. Finally, we have computed the γ -ray flux originated from

the self annihilation of the dark matter candidate S into $b\bar{b}$ final state at the Galactic Centre region. We find that our two component dark matter model also shows an excess in the γ -ray spectrum obtained from the GC region at an energy range $1 \sim 3$ GeV from the annihilation of dark matter candidate S , having mass in the range $30 \sim 40$ GeV. The resulting γ -ray flux becomes lower as the mass splitting between the two dark matter components increases. In the end, we conclude that the γ -ray fluxes computed for $M_\psi = 60$ GeV and 80 GeV with $M_S = 35$ GeV and $\langle\sigma v_{S S^\dagger \rightarrow b\bar{b}}\rangle' \sim (1.52 - 1.67) \times 10^{-26}$ cm³/s agree well with the Fermi-LAT data. Moreover the γ -ray fluxes for $M_\psi \geq 100$ GeV are incompatible with the experimental data. Finally, we have compared the range of allowed values of annihilation cross section with the limits reported by both the Fermi-LAT and DES collaborations. We have found that the range of annihilation cross section for the $b\bar{b}$ annihilation channel predicted from this present model is in right ballpark with reported limits on $\langle\sigma v_{b\bar{b}}\rangle$ by the Fermi-LAT and DES collaborations.

7 Acknowledgements

Author would like to thank D. Adak, A. Dutta Banik and D. Majumdar for many useful suggestions and discussions. Author would also like to acknowledge Department of Atomic Energy (DAE), Govt. of India for their financial assistance.

References

- [1] G. Jungman, M. Kamionkowski, and K. Griest, *Supersymmetric dark matter*, *Phys. Rept.* **267** (1996) 195–373, [[hep-ph/9506380](#)].
- [2] G. Bertone, D. Hooper, and J. Silk, *Particle dark matter: Evidence, candidates and constraints*, *Phys. Rept.* **405** (2005) 279–390, [[hep-ph/0404175](#)].
- [3] L. Goodenough and D. Hooper, *Possible Evidence For Dark Matter Annihilation In The Inner Milky Way From The Fermi Gamma Ray Space Telescope*, [[arXiv:0910.2998](#)].
- [4] D. Hooper and L. Goodenough, *Dark Matter Annihilation in The Galactic Center As Seen by the Fermi Gamma Ray Space Telescope*, *Phys. Lett.* **B697** (2011) 412–428, [[arXiv:1010.2752](#)].
- [5] A. Boyarsky, D. Malyshev, and O. Ruchayskiy, *A comment on the emission from the Galactic Center as seen by the Fermi telescope*, *Phys. Lett.* **B705** (2011) 165–169, [[arXiv:1012.5839](#)].

- [6] D. Hooper and T. Linden, *On The Origin Of The Gamma Rays From The Galactic Center*, *Phys. Rev.* **D84** (2011) 123005, [[arXiv:1110.0006](#)].
- [7] K. N. Abazajian and M. Kaplinghat, *Detection of a Gamma-Ray Source in the Galactic Center Consistent with Extended Emission from Dark Matter Annihilation and Concentrated Astrophysical Emission*, *Phys. Rev.* **D86** (2012) 083511, [[arXiv:1207.6047](#)].
- [8] D. Hooper and T. R. Slatyer, *Two Emission Mechanisms in the Fermi Bubbles: A Possible Signal of Annihilating Dark Matter*, *Phys. Dark Univ.* **2** (2013) 118–138, [[arXiv:1302.6589](#)].
- [9] K. N. Abazajian, N. Canac, S. Horiuchi, and M. Kaplinghat, *Astrophysical and Dark Matter Interpretations of Extended Gamma-Ray Emission from the Galactic Center*, *Phys. Rev.* **D90** (2014) 023526, [[arXiv:1402.4090](#)].
- [10] T. Daylan, D. P. Finkbeiner, D. Hooper, T. Linden, S. K. N. Portillo, et al., *The Characterization of the Gamma-Ray Signal from the Central Milky Way: A Compelling Case for Annihilating Dark Matter*, *Phys. Dark Univ.* **12** (2016) 1-23, [[arXiv:1402.6703](#)].
- [11] *Fermi Science Support Center*, <http://fermi.gsfc.nasa.gov/ssc/data/acess/>, .
- [12] **Fermi-LAT** Collaboration, W. B. Atwood et al., *The Large Area Telescope on the Fermi Gamma-ray Space Telescope Mission*, *Astrophys. J.* **697** (2009) 1071–1102, [[arXiv:0902.1089](#)].
- [13] M. Boucenna and S. Profumo, *Direct and Indirect Singlet Scalar Dark Matter Detection in the Lepton-Specific two-Higgs-doublet Model*, *Phys. Rev.* **D84** (2011) 055011, [[arXiv:1106.3368](#)].
- [14] J. Ruiz-Alvarez, C. de S. Pires, F. S. Queiroz, D. Restrepo, and P. Rodrigues da Silva, *On the Connection of Gamma-Rays, Dark Matter and Higgs Searches at LHC*, *Phys. Rev.* **D86** (2012) 075011, [[arXiv:1206.5779](#)].
- [15] A. Alves, S. Profumo, F. S. Queiroz, and W. Shepherd, *The Effective Hooperon*, *Phys. Rev.* **D90** (2014) 115003, [[arXiv:1403.5027](#)].
- [16] A. Berlin, D. Hooper, and S. D. McDermott, *Simplified Dark Matter Models for the Galactic Center Gamma-Ray Excess*, *Phys. Rev.* **D89** (2014) 115022, [[arXiv:1404.0022](#)].
- [17] P. Agrawal, B. Batell, D. Hooper, and T. Lin, *Flavored Dark Matter and the Galactic Center Gamma-Ray Excess*, *Phys. Rev.* **D90** (2014) 063512, [[arXiv:1404.1373](#)].

- [18] E. Izaguirre, G. Krnjaic, and B. Shuve, *The Galactic Center Excess from the Bottom Up*, *Phys. Rev.* **D90** (2014) 055002, [[arXiv:1404.2018](#)].
- [19] D. Cerdeño, M. Peiró, and S. Robles, *Low-mass right-handed sneutrino dark matter: SuperCDMS and LUX constraints and the Galactic Centre gamma-ray excess*, *JCAP* **1408** (2014) 005, [[arXiv:1404.2572](#)].
- [20] S. Ipek, D. McKeen, and A. E. Nelson, *A Renormalizable Model for the Galactic Center Gamma Ray Excess from Dark Matter Annihilation*, *Phys. Rev.* **D90** (2014) 055021, [[arXiv:1404.3716](#)].
- [21] C. Boehm, M. J. Dolan, and C. McCabe, *A weighty interpretation of the Galactic Centre excess*, *Phys. Rev.* **D90** (2014) 023531, [[arXiv:1404.4977](#)].
- [22] P. Ko, W.-I. Park, and Y. Tang, *Higgs portal vector dark matter for GeV scale γ -ray excess from galactic center*, *JCAP* **1409** (2014) 013, [[arXiv:1404.5257](#)].
- [23] M. Abdullah, A. DiFranzo, A. Rajaraman, T. M. Tait, P. Tanedo, et al., *Hidden On-Shell Mediators for the Galactic Center Gamma-Ray Excess*, *Phys. Rev.* **D90** (2014) 035004, [[arXiv:1404.6528](#)].
- [24] D. K. Ghosh, S. Mondal, and I. Saha, *Confronting the Galactic Center Gamma Ray Excess With a Light Scalar Dark Matter*, *JCAP* **1502** (2015) 035, [[arXiv:1405.0206](#)].
- [25] A. Martin, J. Shelton, and J. Unwin, *Fitting the Galactic Center Gamma-Ray Excess with Cascade Annihilations*, *Phys. Rev.* **D90** (2014) 103513, [[arXiv:1405.0272](#)].
- [26] L. Wang, X. F. Han, *A simplified 2HDM with a scalar dark matter and the galactic center gamma-ray excess*, *Phys. Lett.* **B739** (2014) 416-420, [[arXiv:1406.3598](#)].
- [27] T. Basak and T. Mondal, *Class of Higgs-portal Dark Matter models in the light of gamma-ray excess from Galactic center*, *Phys. Lett.* **B744** (2015) 208-212, [[arXiv:1405.4877](#)].
- [28] W. Detmold, M. McCullough, and A. Pochinsky, *Dark Nuclei I: Cosmology and Indirect Detection*, *Phys. Rev.* **D90** (2014) 115013, [[arXiv:1406.2276](#)].
- [29] C. Arina, E. Del Nobile, and P. Panci, *Not so Coy Dark Matter explains DAMA (and the Galactic Center excess)*, *Phys. Rev. Lett.* **114** (2015) 011301 [[arXiv:1406.5542](#)].

- [30] N. Okada and O. Seto, *Galactic center gamma ray excess from two Higgs doublet portal dark matter*, *Phys. Rev.* **D90** (2014) 083523, [arXiv:1408.2583].
- [31] K. Ghorbani, *Fermionic dark matter with pseudo-scalar Yukawa interaction*, *JCAP* **1501** (2015) 015, [arXiv:1408.4929].
- [32] A. D. Banik and D. Majumdar, *Low Energy Gamma Ray Excess Confronting a Singlet Scalar Extended Inert Doublet Dark Matter Model*, *Phys. Lett.* **B743** (2015) 420-427, [arXiv:1408.5795].
- [33] P. Agrawal, B. Batell, P. J. Fox, and R. Harnik, *WIMPs at the Galactic Center*, *JCAP* **1505** (2015) 011, [arXiv:1411.2592].
- [34] F. Calore, I. Cholis, C. McCabe, and C. Weniger, *A Tale of Tails: Dark Matter Interpretations of the Fermi GeV Excess in Light of Background Model Systematics*, *Phys. Rev.* **D91** (2015) 063003, [arXiv:1411.4647].
- [35] A. Biswas, D. Majumdar, and P. Roy, *Nonthermal Two Component Dark Matter Model for Fermi-LAT γ -ray excess and 3.55 keV X-ray Line*, *JHEP* **1504** (2015) 065, [arXiv:1501.02666].
- [36] Q.-H. Cao, E. Ma, J. Wudka, and C.-P. Yuan, *Multipartite dark matter*, [arXiv:0711.3881].
- [37] S. Profumo, K. Sigurdson, and L. Ubaldi, *Can we discover multi-component WIMP dark matter?*, *JCAP* **0912** (2009) 016, [arXiv:0907.4374].
- [38] D. Feldman, Z. Liu, P. Nath, and G. Peim, *Multicomponent Dark Matter in Supersymmetric Hidden Sector Extensions*, *Phys. Rev.* **D81** (2010) 095017, [arXiv:1004.0649].
- [39] M. Aoki, M. Duerr, J. Kubo, and H. Takano, *Multi-Component Dark Matter Systems and Their Observation Prospects*, *Phys. Rev.* **D86** (2012) 076015, [arXiv:1207.3318].
- [40] A. Biswas, D. Majumdar, A. Sil, and P. Bhattacharjee, *Two Component Dark Matter : A Possible Explanation of 130 GeV γ - Ray Line from the Galactic Centre*, *JCAP* **1312** (2013) 049, [arXiv:1301.3668].
- [41] S. Bhattacharya, A. Drozd, B. Grzadkowski, and J. Wudka, *Two-Component Dark Matter*, *JHEP* **1310** (2013) 158, [arXiv:1309.2986].

- [42] L. Bian, R. Ding, and B. Zhu, *Two Component Higgs-Portal Dark Matter*, *Phys. Lett.* **B728** (2014) 105-113, [arXiv:1308.3851].
- [43] H.-S. Lee and M. Sher, *Dark Two Higgs Doublet Model*, *Phys. Rev.* **D87** (2013) 115009, [arXiv:1303.6653].
- [44] **Planck** Collaboration, P. Ade et al., *Planck 2013 results. XVI. Cosmological parameters*, *Astron. Astrophys.* **571** (2014) A16, [arXiv:1303.5076], P. Ade et al., *Planck 2015 results. XIII. Cosmological parameters* [arXiv:1502.01589].
- [45] **XENON100** Collaboration, E. Aprile et al., *Dark Matter Results from 225 Live Days of XENON100 Data*, *Phys. Rev. Lett.* **109** (2012) 181301, [arXiv:1207.5988].
- [46] **LUX** Collaboration, D. Akerib et al., *First results from the LUX dark matter experiment at the Sanford Underground Research Facility*, *Phys. Rev. Lett.* **112** (2014) 091303, [arXiv:1310.8214].
- [47] G. Belanger, B. Dumont, U. Ellwanger, J. Gunion, and S. Kraml, *Status of invisible Higgs decays*, *Phys. Lett.* **B723** (2013) 340-347, [arXiv:1302.5694].
- [48] S. Gopalakrishna, S. Jung, and J. D. Wells, *Higgs boson decays to four fermions through an abelian hidden sector*, *Phys. Rev.* **D78** (2008) 055002, [arXiv:0801.3456].
- [49] H. Davoudiasl, H.-S. Lee, and W. J. Marciano, *'Dark' Z implications for Parity Violation, Rare Meson Decays, and Higgs Physics*, *Phys. Rev.* **D85** (2012) 115019, [arXiv:1203.2947].
- [50] **ATLAS** Collaboration, G. Aad et al., *Observation of a new particle in the search for the Standard Model Higgs boson with the ATLAS detector at the LHC*, *Phys. Lett.* **B716** (2012) 1-29, [arXiv:1207.7214].
- [51] **CMS** Collaboration, S. Chatrchyan et al., *Observation of a new boson at a mass of 125 GeV with the CMS experiment at the LHC*, *Phys. Lett.* **B716** (2012) 30-61, [arXiv:1207.7235].
- [52] L.-B. Jia and X.-Q. Li, *Study of a WIMP dark matter model with the updated results of CDMS II*, *Phys. Rev.* **D89** (2014) 035006, [arXiv:1309.6029].
- [53] Y. Mambrini, *Higgs searches and singlet scalar dark matter: Combined constraints from XENON 100 and the LHC*, *Phys. Rev.* **D84** (2011) 115017, [arXiv:1108.0671].

- [54] J. Giedt, A. W. Thomas, and R. D. Young, *Dark matter, the CMSSM and lattice QCD*, *Phys. Rev. Lett.* **103** (2009) 201802, [[arXiv:0907.4177](#)].
- [55] R. Barbieri, L. J. Hall, and V. S. Rychkov, *Improved naturalness with a heavy Higgs: An Alternative road to LHC physics*, *Phys. Rev.* **D74** (2006) 015007, [[hep-ph/0603188](#)].
- [56] M. E. Peskin and T. Takeuchi, *Estimation of oblique electroweak corrections*, *Phys. Rev.* **D46** (1992) 381-409.
- [57] **Particle Data Group** Collaboration, K. A. Olive et al., *Review of Particle Physics*, *Chin. Phys.* **C38** (2014) 090001.
- [58] A. Hook, E. Izaguirre, and J. G. Wacker, *Model Independent Bounds on Kinetic Mixing*, *Adv. High Energy Phys.* **2011** (2011) 859762, [[arXiv:1006.0973](#)].
- [59] **SLD Electroweak Group, DELPHI, ALEPH, SLD, SLD Heavy Flavour Group, OPAL, LEP Electroweak Working Group, L3** Collaboration, S. Schael et al., *Precision electroweak measurements on the Z resonance*, *Phys. Rept.* **427** (2006) 257-454, [[hep-ex/0509008](#)].
- [60] P. Ko, Y. Omura, and C. Yu, *Higgs phenomenology in Type-I 2HDM with U(1)-H Higgs gauge symmetry*, *JHEP* **01** (2014) 016, [[arXiv:1309.7156](#)].
- [61] K. Babu, C. F. Kolda, and J. March-Russell, *Implications of generalized Z - Z-prime mixing*, *Phys. Rev.* **D57** (1998) 6788-6792, [[hep-ph/9710441](#)].
- [62] **Gfitter Group** Collaboration, M. Baak, J. Cúth, J. Haller, A. Hoecker, R. Kogler, K. Mönig, M. Schott, and J. Stelzer, *The global electroweak fit at NNLO and prospects for the LHC and ILC*, *Eur. Phys. J.* **C74** (2014) 3046, [[arXiv:1407.3792](#)].
- [63] **ATLAS** Collaboration, G. Aad et al., *Search for high-mass dilepton resonances in pp collisions at $\sqrt{s} = 8$ TeV with the ATLAS detector*, *Phys. Rev.* **D90** (2014) 052005, [[arXiv:1405.4123](#)].
- [64] **CMS** Collaboration, *Search for Resonances in the Dilepton Mass Distribution in pp Collisions at $\sqrt{s} = 8$ TeV*, CMS-PAS-EXO-12-061 (2013).
- [65] J. M. Cline, G. Dupuis, Z. Liu, and W. Xue, *The windows for kinetically mixed Z'-mediated dark matter and the galactic center gamma ray excess*, *JHEP* **08** (2014) 131, [[arXiv:1405.7691](#)].

- [66] **CMS** Collaboration, *Combination of standard model Higgs boson searches and measurements of the properties of the new boson with a mass near 125 GeV*, CMS-PAS-HIG-13-005 (2013).
- [67] G. Belanger and J.-C. Park, *Assisted freeze-out*, *JCAP* **1203** (2012) 038, [[arXiv:1112.4491](#)].
- [68] P. Gondolo and G. Gelmini, *Cosmic abundances of stable particles: Improved analysis*, *Nucl. Phys.* **B360** (1991) 145-179.
- [69] M. Srednicki, R. Watkins, and K. A. Olive, *Calculations of Relic Densities in the Early Universe*, *Nucl. Phys.* **B310** (1988) 693.
- [70] J. Edsjo and P. Gondolo, *Neutralino relic density including coannihilations*, *Phys. Rev.* **D56** (1997) 1879-1894, [[hep-ph/9704361](#)].
- [71] A. Biswas and D. Majumdar, *The Real Gauge Singlet Scalar Extension of Standard Model: A Possible Candidate of Cold Dark Matter*, *Pramana* **80** (2013) 539-557, [[arXiv:1102.3024](#)].
- [72] M. Cirelli, G. Corcella, A. Hektor, G. Hutsi, M. Kadastik, et al., *PPPC 4 DM ID: A Poor Particle Physicist Cookbook for Dark Matter Indirect Detection*, *JCAP* **1103** (2011) 051, [[arXiv:1012.4515](#)].
- [73] J. F. Navarro, C. S. Frenk, and S. D. White, *A Universal density profile from hierarchical clustering*, *Astrophys. J.* **490** (1997) 493-508, [[astro-ph/9611107](#)].
- [74] K. Kong and J.-C. Park, *Bounds on dark matter interpretation of Fermi-LAT GeV excess*, *Nucl. Phys.* **B888** (2014) 154-168, [[arXiv:1404.3741](#)].
- [75] **Fermi-LAT** Collaboration, M. Ackermann et al., *Searching for Dark Matter Annihilation from Milky Way Dwarf Spheroidal Galaxies with Six Years of Fermi-LAT Data*, *Phys. Rev. Lett.* **115** (2015) 231301, [[arXiv:1503.02641](#)].
- [76] **DES, Fermi-LAT** Collaboration, A. Drlica-Wagner et al., *Search for Gamma-Ray Emission from DES Dwarf Spheroidal Galaxy Candidates with Fermi-LAT Data*, *Astrophys. J.* **809** (2015) L4, [[arXiv:1503.02632](#)].
- [77] J. Einasto, *On the construction of a composite model for the galaxy and on the determination of the system of galactic parameters*, *Trudy Inst. Astrofiz. Alma-Ata* **5** (1965) 87.

- [78] J. F. Navarro, et al., *The Diversity and Similarity of Cold Dark Matter Halos*, *Mon. Not. Roy. Astron. Soc.* **402** (2010) 21, [[arXiv:0810.1522](#)].